IOWA STATE UNIVERSITY
Digital Repository

2014

Magnetic hysteresis and Barkhausen noise emission analysis of magnetic materials and composites

Neelam Prabhu Gaunkar
Iowa State University

Follow this and additional works at: https://lib.dr.iastate.edu/etd

⟳ Part of the Electrical and Electronics Commons, Electromagnetics and Photonics Commons, Materials Science and Engineering Commons, and the Mechanics of Materials Commons

Magnetic hysteresis and Barkhausen noise emission analysis of magnetic materials and composites

by

Neelam Prabhu Gaunkar

A thesis submitted to the graduate faculty

in partial fulfillment of the requirements for the degree of

MASTER OF SCIENCE

Major: Electrical and Computer Engineering

Program of Study Committee:

David C. Jiles, Major Professor

Nicola Bowler

Meng Lu

Nathan Neihart

Iowa State University

Ames, Iowa

2014

TABLE OF CONTENTS

LIST OF TABLES

LIST OF FIGURES

ACKNOWLEDGEMENTS

ABSTRACT

Barkhausen emission studies have been used to analyze the effect of residual stresses in ferromagnetic materials. The stresses generated due to mechanical wear and tear, abrasion and prolonged use can also lead to phase changes within the material. These phase changes can cause damage to the structural parts and should be prevented. In this study we analyze the magnetic hysteresis and Barkhausen noise profile of materials with more than one ferromagnetic phase. The correlation between the hysteresis and Barkhausen noise profiles for such materials is studied. Secondary Barkhausen emission peaks can be simulated for such materials. Experimental observations are compared with simulation measurements. Drawing a correlation between the secondary emergent peaks and the composition of each secondary phase should lead to an improved technique for non-destructive characterization of ferromagnetic materials.

Improved sensor-to-specimen coupling is also essential for conducting Barkhausen noise measurements of multiphase materials which may also have different surface geometries. A finite element study was conducted to optimize the design parameters of the magnetizing core in a Barkhausen noise sensor. Several sensor parameters inclusive of core material, core-tip curvature, core length and pole spacing were studied. A procedure for developing a high sensitivity Barkhausen noise sensor by design optimization based on finite element simulations has been demonstrated. The study also shows the applicability of Barkhausen emission and magnetic hysteresis analysis as advanced tools of non-destructive characterization of ferromagnetic materials.

CHAPTER 1.   INTRODUCTION

Electromagnetic methods of Non-Destructive Testing (NDT) and evaluation are increasingly being used for characterization of ferromagnetic materials. Detection and characterization of flaws and in-service microstructural changes in materials are essential aspects of non-destructive evaluation. This can help in the evaluation of integrity of equipment and structures, in addition to assessing the time they can still be used. Magnetic measurements, such as Barkhausen noise and magnetic hysteresis allow testing of ferromagnetic materials in a non-destructive way. These tests are sensitive to stress and microstructural states in materials. The applicability of any NDT technique largely depends on the sensitivity and resolution of the measurement, and on the ability to establish relationship between the measured quantity and behavior of the materials in different conditions. The measurements are also influenced by the design of a sensor employed for the detection and measurement of the signals generated in the material.

1.1   Research Objectives

To develop a non-destructive evaluation technique based on Barkhausen emission analysis. In order to do this it is important to understand the relation between Barkhausen noise emissions and the structure of the material at a microscopic level. The goal of this research is to use the relationship between Barkhausen emission and the microstructure of composite ferromagnetic materials as a non-destructive evaluation tool. This work also focuses on designing suitably efficient sensors for detecting Barkhausen emissions. This is important considering that the emissions are already noise-like.

1.2   Research Motivation

Composite ferromagnetic materials with multiple magnetic phases are increasingly being used in applications such as magnetic data storage, magnetic sensors and actuators, and exchange-spring magnets. These materials occur in single or multiphase conditions and can undergo phase changes during processing or when being used in an application. Such phase changes can affect the performance of the material in applications and in some cases can lead to catastrophic failure. It is therefore important to detect these changes in order to take action to mitigate such failures. Since the changes typically affect the microstructure, and the magnetic properties of these materials are sensitive to changes in microstructure, this research seeks to use Barkhausen emissions as means of evaluating the structural state of the materials. In addition, sensitivity of the sensors for detecting the Barkhausen signals is important both for capturing high quality signals and correctly correlating them to the microstructural conditions of the materials. This is because detected Barkhausen emissions typically originate on the surface of a test specimen as voltage signals and can be captured using inductive sensors. Since the effectiveness of non-destructive evaluation of ferromagnetic components and structures using Barkhausen emissions is strongly dependent on the coupling between the test specimen and the magnetic flux generated by the probe, good coupling allows for improved accuracy in the detecting changes in microstructure and local stress states in the materials; hence providing non-destructive evaluation capability. Consequently, efficient and sufficiently sensitive magnetic Barkhausen emission sensors are crucial.

The design of the existing Barkhausen noise sensor is studied using finite element simulations. This is useful for improving the design of the sensor which in turn is useful for monitoring the structural integrity of ferromagnetic components and structures non-destructively using Barkhausen noise emission technique. The Barkhausen noise profiles for materials with single and dual magnetic phases are also analyzed. It is observed that the presence of a second phase in these materials may be detected with the help of Barkhausen noise signals due to the occurrence of additional peaks in the Barkhausen voltage envelope obtained by linear summation of the individual phases. This behavior in the magnetic response can serve as a tool

for non-destructive testing and evaluation of ferromagnetic parts in which phase constitution and phase changes affect the performance. Thus we conclude that modeling hysteresis and Barkhausen effect in multi-phase ferromagnetic materials is crucial especially due to the need to develop high performance composite magnetic structures.

1.3   Organization of the thesis

Chapter 2 describes the mechanism of magnetic hysteresis. A brief background of the different hysteresis models is presented followed by a detailed discussion on the Jiles-Atherton model of hysteresis.

Chapter 3 discusses the use of Barkhausen noise emissions as a tool for non-destructive evaluation of materials. A stochastic model of the Barkhausen effect is described in detail. The chapter also focuses on design considerations of a sensor for Barkhausen emission measurement. Optimization of magnetization core parameters using finite element analysis is presented. The finite element analysis details the optimum design under quasi-static conditions.

Chapters 4 and 5 integrate magnetic hysteresis measurements and Barkhausen emission analysis as NDE tools for analyzing and evaluating the microstructural state of ferromagnetic materials. Microstructure, crystal structure, magnetic properties and Barkhausen emission profiles were studied for materials containing a single ferromagnetic phase and two ferromagnetic phases. An extension to the Jiles-Atherton model to accommodate materials with two ferromagnetic phases is also presented.

Chapter 6 highlights the conclusions from this research. Several directions for future work in the areas of hysteresis modeling, Barkhausen noise analysis and multiphase material analysis are suggested.

CHAPTER 2. MAGNETIZATION AND HYSTERESIS BEHAVIOR IN FERROMAGNETIC MATERIALS

2.1 Magnetic Hysteresis

When the magnetic field applied to ferromagnetic materials is cycled in time, the magnetization does not trace its initial path, resulting in magnetic hysteresis. This hysteretic behavior is related to the influence of the applied magnetic field on magnetic moments which are aligned in particular crystallographic directions in different regions in the material. Such regions are known as magnetic domains and the crystallographic directions in which the moments align are called easy magnetization directions. In neighboring domains, the moments within each domain are aligned along different directions as seen in Fig. 2.1 (left). The interfaces between adjacent domains (called the domain wall) can be a few hundred atomic layers thick or even a few atoms (based on the material) and the orientations of the moments change progressively within these layers from that of one domain to that of another. When an external magnetic field is applied to a ferromagnetic material, as in Fig. 2.1 (right), at magnetic field strengths sufficient to move the domains past any pinning sites, the magnetic moments within each domain then switch to crystallographic easy directions closest to their orientation. With sufficient field to overcome
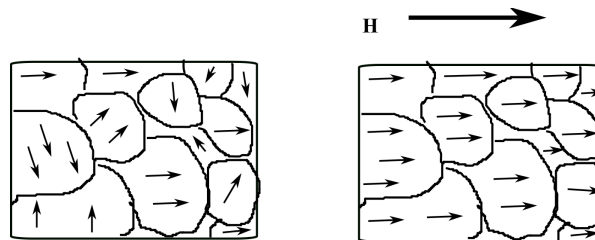
Figure 2.1   Schematic illustration of magnetic domains within grains. The arrows represent the magnetic moments which are randomly oriented before magnetization (left) and are oriented along the direction of external magnetic field (right)

the anisotropy energy, they switch to the direction of applied magnetic field to attain a state of minimum energy [Jiles and Atherton (1986); Bertotti (1998)]. During the magnetization process, the domains oriented in the direction of the external field (favorably oriented domains) grow at the expense of neighboring less favorably oriented ones; which shrink. The presence of imperfections or defects within the material serve as a source of lag during magnetization by acting as pinning sites to the domain walls. At sufficiently high magnetic field strengths, all domains will become oriented to the direction of applied field. A sufficiently strong magnetic field can even reorient the magnetic moments oriented along favorable crystallographic direction in the direction of the applied magnetic field. Beyond this, no further magnetization is possible and the material is then said to be saturated. If the direction of magnetic field is reversed, the magnetic moments realign along the favorable crystallographic direction thereby reducing the magnetization mainly because this reduces the total energy of the system. The hysteresis loop is illustrated in Fig. 2.2. The imperfections and impurities in the material affect the shape of the hysteresis loop. Magnetocrystalline anisotropy also influences the hysteresis loop because it affects the ability of domain walls to align along the field direction.

For ferromagnetic materials, the hysteresis process can be described mathematically. If an external magnetic field, H, is applied to a ferromagnetic material with relative permeability of free space, μ_o, the magnetic induction, B, within the material is:

$$B = \mu_o(M + H) \tag{2.1}$$

where M is the magnetization of the ferromagnetic material. On the microscopic level, the hysteresis process can be divided into the following processes [Jiles (1998)].

- In a demagnetized state, the magnetic moments are randomly oriented such that the net magnetization is zero

- At saturation, all the magnetic moments align in the direction of the applied magnetic field

- The magnetization which remains after removal of the externally applied magnetic field is known as the remanent magnetization as observed in Fig. 2.2
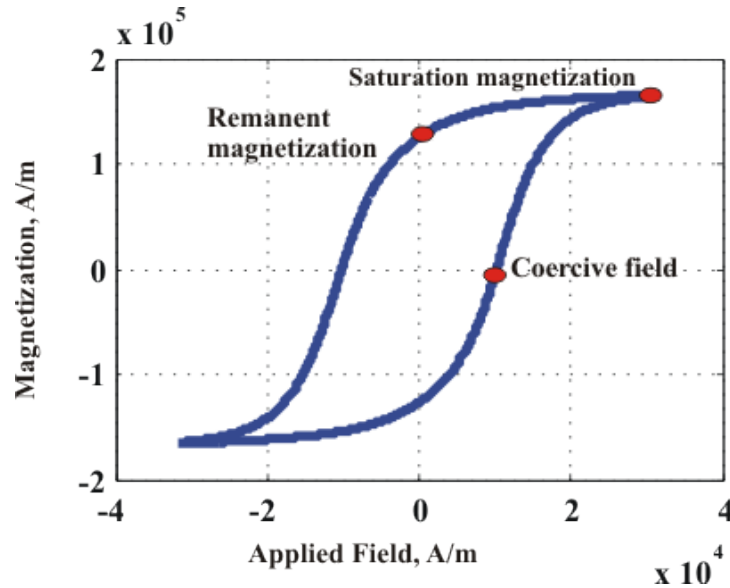
Figure 2.2   Illustration of magnetization process

• The magnetic field when the net magnetization is zero is known as the coercive field as seen in Fig. 2.2

Describing the hysteresis loop allows for predicting the magnetic properties such as the coercivity or remanence for magnetic materials and in turn allows for improving their performance in devices. Historically, several models have been proposed to predict this hysteresis behavior. Some earlier work suggested a frictional force responsible for hysteresis and others considered hysteresis as a byproduct of the interactions between the magnetic moments [Jiles and Atherton (1986)]. It is now understood that both of these physical phenomena contribute to hysteresis. The apparently smooth nature of the hysteresis loop is attributed to a frictional force opposing the change in magnetization. This is due to the pinning of domain walls by defects in specimens which cause an opposing force resisting changes in magnetization. The mutual interactions between the magnetic domains are also contributing factors and will be described in detail in section 2.3.

The next section describes the different magnetic hysteresis models.

2.2   Models to predict magnetic hysteresis

Several models have been developed to characterize magnetic hysteresis. The well known models include the Landau -Lifshitz [Landau (1935)], Preisach [Preisach (1935)], Stoner-Wohlfarth [Stoner (1948)] and the Jiles-Atherton [Jiles and Atherton (1986)] model.

2.2.1   Landau-Lifshitz Model

The Landau-Lifshitz model was proposed to describe the time-domain behavior of magnetic moments under the influence of externally applied magnetic field [Landau (1935)]. On the macroscopic scale, it can be said that magnetic moments rotate under the influence of an external magnetic field. The model applied the same principle at a microscopic scale and the behavior of the bulk material is determined by integrating the rotation over the entire volume. Computation over the individual magnetic moments requires large processing time and thus limits the application of this model to our study.

2.2.2   Preisach Model

The Preisach model follows a macroscopic approach [Preisach (1935)]. The ferromagnetic material is considered to comprise of small domains each magnetized to a value of either $+m$ or $-m$, where m corresponds to the magnetization. The model assumes each domain to have the same magnetization and varying switching fields. Since the model lays importance on the switching characteristics, it can be applied to any system exhibiting hysteresis. The mathematical approach inhibits us from relating the material characteristics to the response and thus the Preisach model is not particularly suited for this study.

2.2.3   Stoner-Wohlfarth Model

The Stoner-Wohlfarth model [Stoner (1948)] describes magnetic hysteresis in terms of synchronous rotation of single-domain particles or magnetic moments. The original form of this model makes no provision for magnetic interactions between the domains. The model relies on the effect of anisotropy to determine how magnetic domains behave in the presence of an

external magnetic field. The model finds applications in determining the magnetization characteristics of magnetic particles in recording media.

2.2.4 Jiles-Atherton (J-A) Model

The Jiles-Atherton (J-A) model [Jiles and Atherton (1986)] considers a magnetized material to be an array of distributed magnetic moments subjected to a magnetic field. The total magnetization of the material is found by integrating the distribution of magnetic moments over all orientations. The model incorporates effects of anisotropy and coupling between the individual domains. Compared to the other hysteresis models which describe hysteresis in terms of domain rotation or switching, the Jiles-Atherton Model describes hysteresis in terms of domain wall motion thus enabling a connection to the physical response of the magnetic material. A comparison of the different models is found in Table 2.1 [Raghunathan (2010); Liorzou et al. (2000)]. Of the available empirical models, the Jiles-Atherton (J-A) model [Jiles and Atherton (1986)] and the Preisach model [Preisach (1935)] are widely used. Since the Preisach model requires a relatively higher computation time in contrast to the J-A model, for this study, we adopted the J-A model to study hysteresis in ferromagnetic two-phase materials.

Table 2.1   Different models of magnetic hysteresis [Raghunathan (2010); Liorzou et al. (2000)]

Features	Landau-Lifshitz	Preisach	Stoner-Wohlfarth	Jiles-Atherton
Mechanism	rotation	switching	rotation	domain wall motion
Interaction	yes	no	yes	yes
Number of Parameters	3	3	4	5
Pinning	no	not specified	yes	yes
Run-time	very large	average	average	low

2.3   Original form of J-A model for magnetic hysteresis

The underlying phenomena of domain wall bending and domain wall translation are incorporated in the Jiles-Atherton model of hysteresis. It describes the magnetic hysteresis considering the impedances to domain wall motion due to uniformly distributed pinning sites. The total work done in moving the magnetic domain against the pinning sites is proportional to the change in magnetization. In the J-A model an array of distributed magnetic moments is con-

sidered to be in thermal equilibrium at a particular temperature. The bulk magnetization of the material is then obtained by integrating the magnetization over all the magnetic moments in all possible orientations.

Five physical material characteristics emerge from the model including the spontaneous magnetization (M_s), the domain coupling parameter (α), the domain density (a), the reversibility factor (c) and pinning factor (k). These parameters are also known as the Jiles-Atherton model parameters. The contribution of these parameters in describing magnetic hysteresis is further discussed.

1. Spontaneous Magnetization (M_s): The magnetization state when all the magnetic domains are aligned parallel is known as spontaneous magnetization. However, when the external magnetic field is increased slowly, the magnetization increases very slowly to reach technical saturation. This increase is attributed to increase in spontaneous magnetization within a single domain. The magnetic domains which are not perfectly aligned with the field due to thermal energy are completely aligned at this point.

2. Domain Coupling factor (α): The domain coupling factor is a parameter that represents the mean field coupling between the domains. It is related to the remanence and the permeability of the material.

3. Domain density factor (a): The domain density factor corresponds to the number of magnetic domains within the material. This factor influences the slope of the hysteresis curve and thus corresponds as a measure of permeability of the material.

4. Reversibility factor (c): The reversibility factor is a representation of the reversible magnetization component. When an external magnetic field is applied to the ferromagnetic material, the magnetic moments align in the direction of the applied field. On removing the external field, the moments revert to their original orientations.

5. Pinning factor (k): The pinning factor is proportional to the pinning site energy and the pinning site density. The pinning site energy primarily determines the coercivity. This leads to irreversible behavior.

The parts of the hysteresis loop represented by the J-A model parameters are schematically shown in Fig. 2.3.

Incorporating these five parameters in the Jiles-Atherton model equation enables complete description of the hysteresis curve including the underlying physical phenomena.
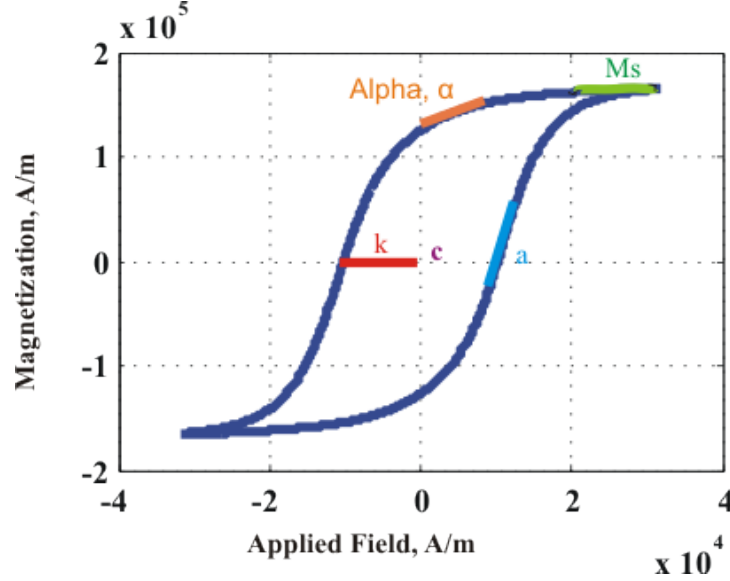
Figure 2.3   Schematic illustration of Jiles-Atherton model parameters

A modified form of the Langevin expression as seen in 2.2 is used to describe the steady anhysteretic state or ideal magnetization process. This state corresponds to the case where there are no impedance's to the change in magnetization and cannot be practically realized. Equation 2.2 highlights the dependence of the anhysteretic magnetization M_{an} on the saturation magnetization M_s, the domain density a and the effective field H_e.

$$M_{an} = M_s\Big(coth\Big(\frac{H_e}{a}\Big) - \Big(\frac{a}{H_e}\Big)\Big) \tag{2.2}$$

The effective field is further considered to be a combination of the applied field H and the magnetization M scaled by the coupling parameter α and is described as follows

$$H_e = H + \alpha M \tag{2.3}$$

Practically, the changes in magnetization can be subdivided into the magnetic domain processes which contribute to net reversible and irreversible changes in magnetization.

M refers to the total magnetization which can be further subdivided into the irreversible and reversible magnetization as seen in 2.4.

$$M = M_{irr} + M_{rev} \tag{2.4}$$

When a domain wall encounters a pinning site as observed in Fig. 2.4, there is an associated loss in energy. It is assumed that the change in energy of a ferromagnet is manifested either as a change in magnetization or as hysteresis loss. The net energy supplied to the material is then described as a summation of change in magnetostatic energy and hysteresis. When there is no hysteresis loss, we can say that the change in magnetostatic energy is equivalent to the energy supplied. This results in anhysteretic magnetization. The irreversible magnetization component is primarily due to domain wall pinning and irreversible rotation. Thus,

$$\frac{dM_{irr}}{dH} = \frac{M_{an}(H) - M_{irr}(H)}{k - \alpha[M_{an}(H) - M_{irr}(H)]} \tag{2.5}$$

The reversible magnetization is attributed to domain wall bowing, reversible translation and
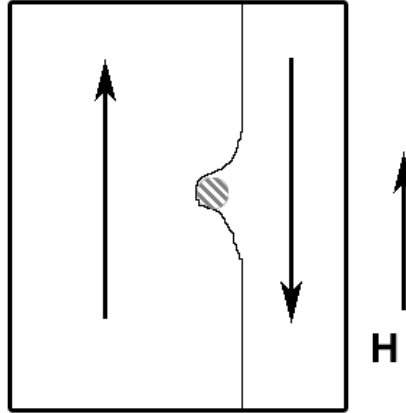
Figure 2.4   Schematic of domain wall encountering a pinning site (Adapted from Wikipedia)

reversible rotation. In the model it takes the form,

$$M_{rev} = c(M_{an} - M_{irr}) \tag{2.6}$$

Equations 2.5 and 2.6 cannot describe all the changes during magnetization beginning from reversible magnetization, pinning of the domain wall and the irreversible magnetization changes. The change in magnetization is a more effective measure of the overall magnetization process. Thus,

$$\frac{dM}{dH} = \frac{dM_{irr}}{dH} + \frac{dM_{rev}}{dH} \tag{2.7}$$

Combining all the relations described, mathematically, the hysteresis behavior can be described using the relation as seen in Equation 2.8.

$$\frac{dM}{dH} = \frac{1}{(1+c)} \frac{M_{an} - M}{\delta k - \alpha(M_{an} - M)} + \frac{c}{(1+c)} \frac{dM_{an}}{dH} \tag{2.8}$$

Here M refers to the total magnetization, M_{an} represents the anhysteretic magnetization, H refers to the applied field and δ the directional parameter, which takes the value +1 when H increases and -1 when H decreases.

A schematic indicating the hysteresis in a single-phase material can be observed in Figure. 2.5. The Jiles-Atherton Model equation allows for a reasonably close match with the measured data. It should be noted that though the hysteresis curves appear smooth, there are localized
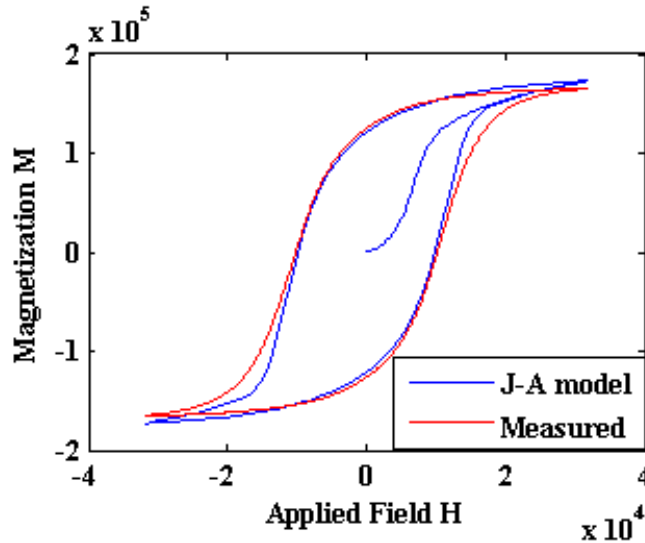
Figure 2.5 Schematic illustration of Jiles-Atherton model [Raghunathan (2010)]

distortions at a microscopic level. These distortions are caused by discontinuous jumps of domain walls during the magnetization process as they interact with pinning points. These

microscopic activities can be observed as Barkhausen noise signals. Interpreting these signals accurately along-with the examination of the hysteresis process can help to relate microscopic and macroscopic activity within ferromagnetic materials and this will be described in detail in Chapter 3.

CHAPTER 3.   MAGNETIC HYSTERESIS AND BARKHAUSEN EMISSIONS

3.1   Background

The Barkhausen Effect was first observed by Heinrich Barkhausen in 1919 and was described as sudden changes in magnetization when a ferromagnetic material is being magnetized on application of a continuously varying (or alternating) magnetic field. This phenomenon is attributed to the interaction of the magnetic domains with pinning sites as the domains favorably aligned in the direction of applied magnetic field grow at the expense of others. Such growth results in the movement of domain walls separating the domains.

The movement of the domain walls past pinning sites results in discontinuous magnetization which leads to Barkhausen jumps. Magnetization plots appear smooth macroscopically but at a microscopic level, the changes in magnetization are observed to be in incremental steps (discontinuous), as illustrated in Fig. 3.1.
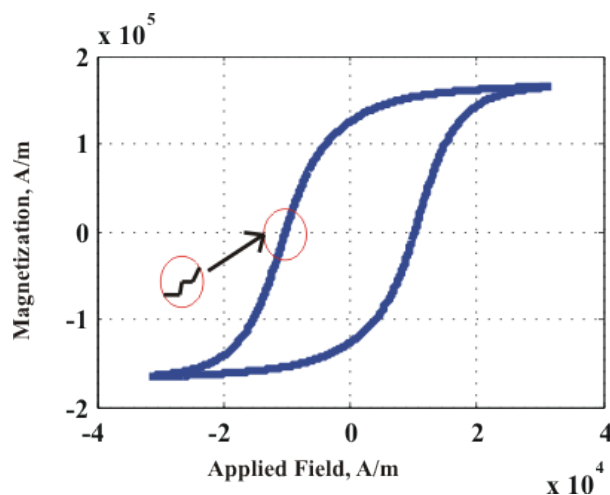
Figure 3.1   Illustration of Barkhausen jumps during magnetization. The jumps are caused by sudden domain wall movements on the microscopic level

There are five main mechanisms due to which magnetic Barkhausen emissions occur [Jiles (1988)]:

1. Discontinuous, irreversible domain wall motion

2. Discontinuous rotation of magnetic moments within a domain

3. Appearance and disappearance of domain walls (Bloch or Neel). Domain walls are narrow transition regions between magnetic domains. They only differ in the plane of rotation of magnetization. For Bloch walls the magnetization rotates through the plane of the domain wall whereas for Neel walls the magnetization rotates within the plane of the domain wall.

4. Inversion of magnetization in single-domain particles

5. Displacement of Bloch or Neel lines in two 180^0 walls with oppositely directed magnetizations

Fig. 3.2(a) highlights a typical profile of the BN signal which is acquired as a voltage signal. As the domain wall moves, electromagnetic waves move outward and are picked up as induced emf in a coil as indicated in Fig. 3.2(b).

(a) Illustration of Barkhausen noise signal

(b) Illustration of EM wave traveling to the sample surface
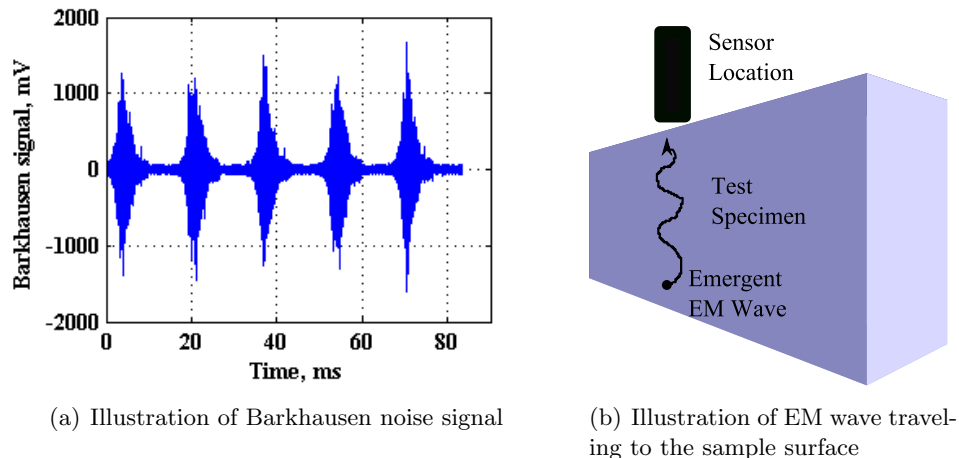
Figure 3.2   (a) Barkhausen noise signal and (b) signal propagation

Mathematically, this induced voltage can be described by Faraday's law of electromagnetic induction which states that a change in magnetic flux corresponds to a change in induced emf.

The power spectrum of magnetic Barkhausen noise emissions extends to about 2 MHz [Kaplan et al. (2007)] and the amplitude may decay exponentially as a function of depth below the surface. The decay can be ascribed to the skin effect due to the emergence of opposing eddy currents. Therefore, an increase in the magnetization frequency is not preferred since the measurement depth is dependent on the signal frequency and material properties such as conductivity and permeability.

Two important material phenomena affect the intensity of the Barkhausen noise signal. One is magnetoelastic interaction due to the presence and distribution of stresses which affects the way domains align during magnetization. As a result of magnetoelastic interaction in materials, stress in ferromagnetic materials can be related to the pulse height of the Barkhausen signal. Compressive stresses tend to result in low amplitude signals whereas tensile stresses result in high amplitude signals [Mierczak et al. (2011)]. Thus, measurement of Barkhausen noise signal amplitude can be used to determine the stress-state of test materials. Changes in the density of dislocations is another phenomenon that also affects the magnetic Barkhausen signals. For some materials the dimensions of magnetic domains and domain walls are comparable to those of phases, grains etc. and therefore the Barkhausen signals may be used to distinguish between microstructures [Roy et al. (2012)].

3.1.1   Barkhausen effect as an NDE tool

Due to the strong coupling between the magnetic properties and microstructural features in ferromagnetic materials [Dimian and Andrei (2014)], Barkhausen effect presents a powerful tool for non-destructively monitoring the condition of such materials. Manufacturing and post-manufacturing treatments of ferromagnetic structures can introduce residual stresses that can ultimately result in structural failure. Barkhausen effect can be used to detect and evaluate the state of such residual stresses in order to initiate the necessary mitigation approaches. This can be done by correlating the peak amplitude of the voltage obtained during Barkhausen emission measurement with stress [Kypris et al. (2012); Mierczak et al. (2011)]. Recent work [Kypris et al. (2013a, 2014)] has focused on correlating the residual stresses with the depth in which they exist in structures. For industrial applications, monitoring of structural health can be

incorporated in the process chain as a quality assurance procedure. Such methods can help to avoid failures resulting from microstructural changes, residual stresses, surface deformations and micro-cracks leading to microscopic cracks and failure.

3.2 Barkhausen noise (BN) detection, monitoring and analysis

Apart from the stress-state or other microstructural inhomogeneities in the materials, the detected Barkhausen signal also depends on the magnetizing field produced by the coils, the core geometry, sensor-to-specimen coupling and spacing between core tips. It is therefore important that the sensor configuration be optimized to improve the sensitivity, reproducibility and accuracy of the detected Barkhausen signals. Using finite element simulations a method of optimizing these parameters for sensors with C-core geometries with two windings is demonstrated. The choice of performing DC simulations and thus ignoring frequency dependent effects is supported by the fact that typical Barkhausen noise excitation coils operate in the lower quasi-static limit (1-100 Hz), and are thus well described by a DC approach. All the simulations were conducted under identical boundary conditions.

3.2.1 Design of BN sensor

From Ampere's circuital law, for a magnetic circuit:

$$\oint \mathbf{H} \cdot d\boldsymbol{\ell} = NI \tag{3.1}$$

Here $\mathbf{H}$ is the magnetic field strength in the core, generated due to current I flowing in a coil having N turns. $\boldsymbol{\ell}$ is the length of the flux path. The equivalent circuit of the magnetizing unit for this study is shown in Fig. 3.3(a). The total magnetic field strength due to the two magnetizing coils is taken to be 0.5 kA/m, in line with a previous study [Kypris et al. (2013b)] on Barkhausen measurement. The two magnetizing coils can be approximated as solenoids of finite lengths. One can therefore find the field intensity along the axis, at a distance x from the center of the solenoid using the relation [Jiles (1998); Umenei et al. (2011)],

$$H = \left[\frac{Ni}{L} \left(\frac{(L + 2x)}{2\sqrt{[D^2 + (L + 2x)^2]}} + \frac{(L - 2x)}{2\sqrt{[D^2 + (L - 2x)^2]}} \right) \right] \tag{3.2}$$

Here D is the coil diameter, which for the C-core under test represents a coil with value shown in Table 3.1. L is the length of the magnetizing coil. The magnetic field at the off-axis point C, which in this study is the center of the test specimen, is considered to be equivalent to the on-axis field at a distance x from the center of the coil. This is a valid approximation since the magnetic flux path is curved by the material, thus making it possible to set x=ABC. Therefore, the relationship described in equation 3.2 can be used to approximate the value of the magnetic field at the point marked C. Since the analytical expression is an approximation of the magnetic field at point C, finite element simulations are utilized for improved accuracy.
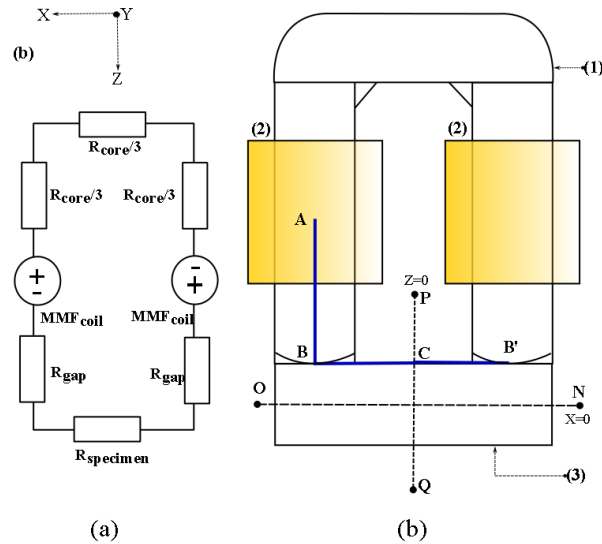
Figure 3.3   (a) The equivalent magnetic circuit. (b) Schematic of the magnetizing assembly showing the core material (1), coils (2) and test specimen (3). Line segments NO and PQ represent sections along X and Z direction respectively. [Gaunkar et al. (2014)]

3.2.2   FEM simulation results of electromagnetic processes

Fig. 3.3(b) shows the geometry of the magnetizing unit. C-core geometry was selected, being a typical geometry for Barkhausen sensors. The number of turns and coil length for the magnetizing coils were calculated using equation 3.5. A DC magnetizing current of 1 A was

assumed. The properties and dimensions of the core and the coil are listed in Table 3.1. A finite element simulation was performed using the AC/DC module of COMSOL Multiphysics.

Table 3.1   Core and Coil Dimensions (Per pole)

Sensor	Coil	Core
Material	Copper	Variable
Length	8mm	14mm
Width	4mm	3.4mm
Depth	4mm	3.4mm
Number of Turns	32	N/A

The effects of using different core materials for the magnetizing unit and the variations in the tip-curvature, length and inter-pole spacing of the core-materials have been investigated.

3.2.2.1   Effect of core material

Table. 3.2 shows the core materials investigated including their electrical and magnetic properties.

Table 3.2   Properties of materials studied as core materials for the magnetizing unit

Material	Electrical Conductivity S/m	Relative Permeability	Relative Permittivity
Air	0	1	1
Iron	1E7	5000 [Chung (2010)]	300 [Wilson (2005)]
78 Permalloy	0.5E7	100000	5000 [Wilson (2005)]
Electrical Steel	2.12E6	4000	1
Ni-Zn Ferrite	2E-5 [Goldman (2005)]	1000 [Lyshevski (2005)]	14 [Goldman (2005)]

It can be seen in Fig. 3.4 that the maximum magnetic flux density in the material corresponds to the material with highest permeability μ_r. Although permalloy has the highest flux concentration, its saturation magnetization (0.86×10^6 A/m) is almost half of that of iron (1.71×10^6 A/m). Since it is important not to saturate the core material in application, iron was selected as the choice material for the rest of the study.
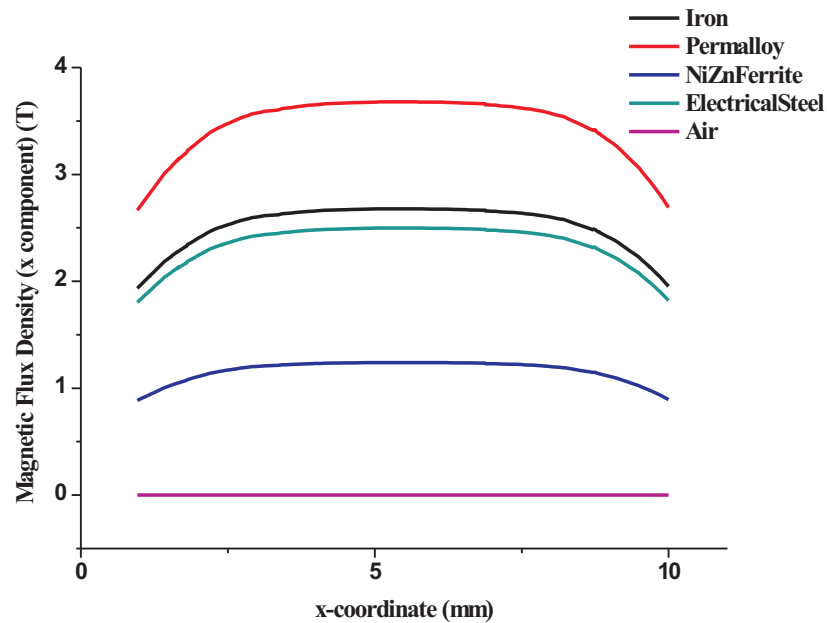
Figure 3.4   Effect of material on magnetic flux density. Magnetic flux density was measured between the pole centers along the line segment NO as seen in Fig. 3.3.(b)

3.2.2.2   Effect of core-tip curvature

A slight curvature as indicated in Fig. 3.3 (b)is introduced and the effect of variation in core-tip curvature on the magnetic flux density in the sample is shown in Fig. 3.5. The curvature of the core-tip is an important parameter to ensure good sensor-to-specimen coupling. Cores with flat, pointed and curved tips were investigated. Fig. 3.5 shows that the best performance can be obtained using a core-material with a flat tip. Nevertheless, in applications, a curved core-tip helps ensure consistent flux coupling with test specimens of varying surface geometries. Hence the core-tip curvature selected has an arc length of 3.45 mm, that is 0.55 mm less than the length of a flat tip. Magnetic flux leakage occurs in the region between the core poles resulting in asymmetrical flux density above and below the test specimen.

3.2.2.3   Effect of core length

The effect of path length of the core material on the generated magnetic field is shown in Fig. 3.6. These are obtained using an iron core with an arc length of 3.45 mm. The magnetic
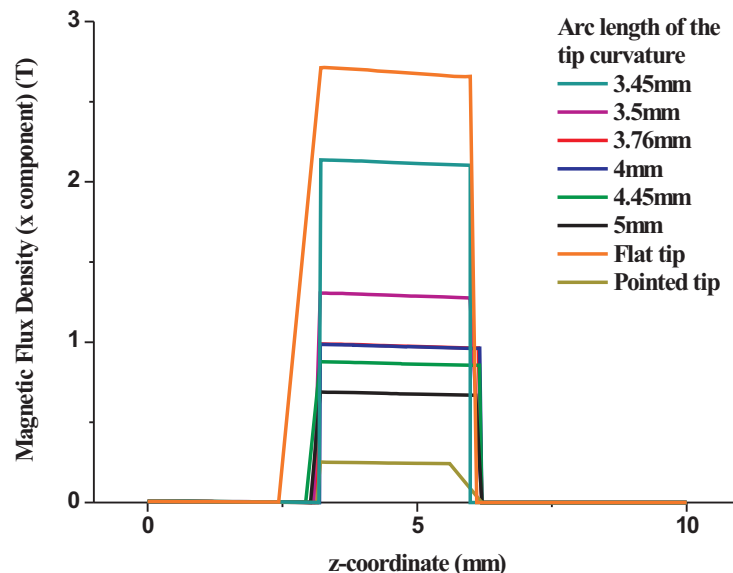
Figure 3.5   Effect of tip curvature on the magnetic flux density. Magnetic flux density was measured along the line segment PQ as shown in Fig. 3.3(b).

field strength decreases with increasing length of the core material. This is an important design consideration especially when varying the sensor size is necessary to test different parts of the same component. The maximum field strengths obtained at point C are in the range 0.31 to 0.4 kA/m. This is less than the calculated value of 0.5 kA/m and might be due to flux leakage. The maximum field penetration is obtained when the magnetizing coils are placed at a distance of 0.5 mm (i.e. closest to the test specimen). This was incorporated into the design to observe the effect of spacing between the poles of the sensor.

3.2.2.4   Effect of inter-pole spacing

Fig. 3.7 shows the effect of varying the spacing between the two poles of the sensor. It can be seen that small spacing maximizes the magnetic flux density. However, in application, maximizing the flux density by decreasing the pole spacing should be balanced with the fact that measurement noise increases due to mutual inductance when the pole spacing is reduced. This is important considering that Barkhausen emissions are already noise-like.

Through this analysis it is understood that several factors contribute to the improved per-
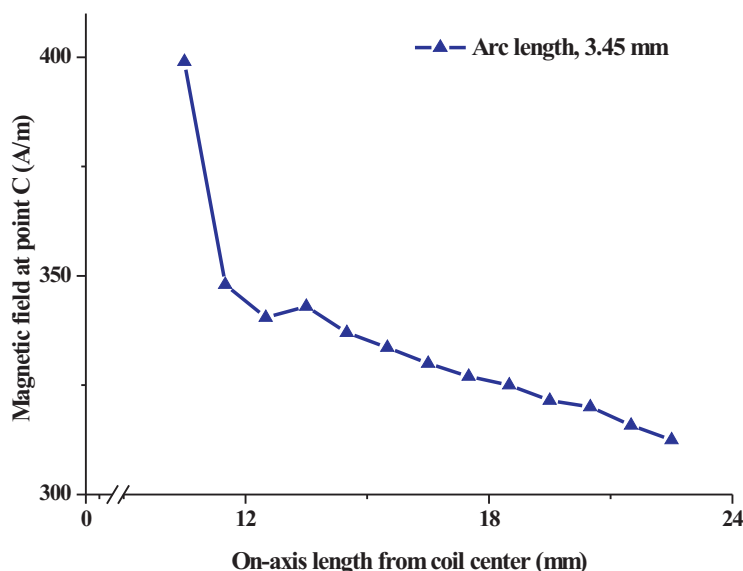
Figure 3.6   Effect of core length on magnetic field. The on-axis length from coil center is defined as the length along path ABC, shown in Fig. 3.3(b). AB varies with increasing length of poles.

formance of the sensor. Since the Barkhausen noise signal is already noise-like and stochastic, higher accuracy and precision in measurement are essential. The stochastic behavior of the Barkhausen noise emissions can be best described by the stochastic model for Barkhausen effect discussed in the following section.

3.3   Stochastic Model for Barkhausen effect

The stochastic nature of the Barkhausen emissions have been studied in detail [Alessandro et al. (1990); Bertotti and Mayergoyz (2006); Jiles (2000)]. Although Barkhausen emissions result from discontinuous magnetization changes inside a material, they can be measured on the surface of the material using an inductive sensor. This interesting feature of magnetic Barkhausen emission (MBE) is utilized and correlated to the magnetization to study the ferromagnetic phases within the material. From Faraday's law of electromagnetic induction the induced emf V_{emf} sensed by the Barkhausen sensor is proportional to the rate of change of magnetic flux with time $d\phi/dt$ which is equivalent to the rate of change of magnetization with
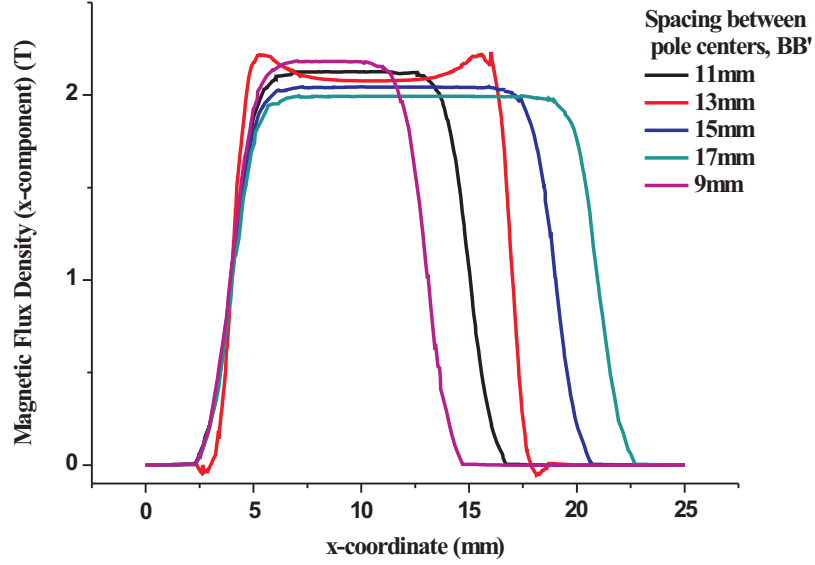
Figure 3.7   Effect of pole spacing. The pole spacing was measured along the line segment NO, as shown in Fig. 3.3(b), where BB' indicates the spacing between the pole centers

time scaled by the area of the pick-up coil and the permeability of free space [Tumanski (2007)]. Alternatively, the sum of the magnetization jumps (jump sum magnetization dM_{JS}/dt) due to the irreversible component of magnetization is related to Barkhausen emissions. The fluctuating nature of Barkhausen emissions is thought to arise from stochastic fluctuations in the local pinning field H_c. In particular, the level of Barkhausen activity is related to irreversible changes in magnetization occuring over a given time interval. The relationship between the induced emf, the time rate of change of M_{JS} and the irreversible magnetization component due to an applied magnetic field is shown in 3.3 where dM_{irr}/dH is the differential susceptibility and dH/dt is the time rate of change of the applied magnetic field [Mitra and Jiles (1995); Jiles et al. (1993)].

$$|V_{emf}| \propto \frac{dM_{JS}}{dt} = \gamma \frac{dM_{irr}}{dH} \frac{dH}{dt} \tag{3.3}$$

Here γ, a dimensionless term, represents the ratio of the discontinuous magnetization M_{disc} to the irreversible component of magnetization M_{irr} multiplied by N_t, the number of Barkhausen events occurring in a given time period. $\langle M_{disc} \rangle$ represents average discontinuous

change in magnetization. In this case it is considered to be an ensemble average. It is also a very small quantity. Numerically [Jiles (2000)],

$$\gamma = \frac{d\langle M_{disc}\rangle N_t}{dM_{irr}} = \langle M_{disc}\rangle \frac{dN_t}{dM_{irr}} + N_t \frac{d\langle M_{disc}\rangle}{dM_{irr}} \tag{3.4}$$

It was found that the size of the Barkhuasen jumps $\langle M_{disc}\rangle$ is considered to be weakly related to the irreversible change in magnetization and thus, γ can be approximated to be equal to $\langle M_{disc}\rangle dN_t/dM_{irr}$. As described by the stochastic Barkhausen model of Bertotti [Bertotti (1983)], the number of Barkhausen events N_t is considered to be a stochastically fluctuating function in a given time interval. The random nature of Barkhausen emissions allows the number of events N_t to be described by a recursive relation wherein the number of events is always held to be a positive, non-zero quantity. The relation is recursive since a correlation exists between the number of events from one time interval to the next. The probability of a Barkhausen event occurring at any given location is low; however, the number of locations is large. Thus, the increment in the number of events with time is assumed to follow a Poisson distribution [Jiles (2000)]. The number of events N_t in the time interval t is related to the number of events N_{t-1} in the previous time interval $t-1$ as seen in 3.5. Since the number of Barkhausen events follows a Poisson distribution the standard deviation of a number of events N_t is equal to $\sqrt{N_t}$.

$$N_t = N_{t-1} + \delta_{rand}\sqrt{N_{t-1}}; \tag{3.5}$$

δ_{rand} is a random number lying in the range $\pm$ 1.47. Originally, δ_{rand} was assumed to lie in the range $\pm$ 1. However 32 % of the time the increment in N_t should be beyond one standard deviation [Jiles (2000)]. Incorporating equations 3.1, 3.4 and 3.5 the Barkhausen activity can be modeled as described by the relation in 3.6.

$$\frac{dM_{JS}}{dt} = \frac{dM_{irr}}{dH}\frac{dH}{dt}\langle M_{disc}\rangle \frac{dN_t}{dM_{irr}} \tag{3.6}$$

In equation 3.6 it is approximated that the number of events N_t is a linear function of M_{irr} and the equation indicates that the magnetization jump sum is proportional to the number

of Barkhausen activities resulting from discontinuous magnetization process. Equations 2.8 and 3.6 form the foundation for the stochastic-hysteretic model for Barkhausen emissions. In the following sections these relations are extended to describe the Barkhausen noise signals in two-phase magnetic materials.

CHAPTER 4.   SINGLE PHASE MATERIAL CHARACTERIZATION

4.1   Background

Several studies have already shown the correlation between the sensitivity of Barkhausen noise and variations in microstructure, phase, stress state and grain size in ferromagnetic materials [Blaow et al. (2006); Raghunathan et al. (2013); Ktena et al. (2014)]. The aim of this study is to investigate the possibility of extending this correlation to first a single phase material and then extending the concept to detection and characterization of multiphase ferromagnetic composite using magnetic Barkhausen noise technique. In this chapter the focus is on single phase material characterization.

Magnetic Barkhausen noise measurement is considered to be a promising non-destructive evaluation technique for microstructural and mechanical characterization of ferromagnetic materials when used with appropriate calibration procedures. Magnetic Barkhausen emissions (MBE) are known to be strongly affected by the domain configuration, mobility of domain walls, density of pinning sites and also depend on microstructural parameters such as grain size, composition, hardness and lattice strains.

It is also known that ferromagnetic materials undergo changes in microstructure, texture, homogeneity, or lattice strains, etc. due to phase transformations, environmental degradation, fatigue loading, creep, stress, corrosion, decarburization and irradiation damage. Since such changes can lead to the degradation of material properties, it is important to detect such changes in order to avoid structural failure. Continuous in-situ monitoring of materials in service is sometimes important in critical equipment and requires their continuous monitoring for the possibility of development of damage and flaws in the material. Being a relatively rapid and economical non-destructive evaluation technique, MBE measurements can provide

an economical and industrially beneficial technique. The Barkhausen parameters are sensitive to a number of material conditions, hence relationships between specific material characteristics are of interest, such as constituent phases, microstructures, localized strains. The applicability of this technique, however, requires understanding of the response of materials to magnetization and the relationship between Barkhausen emission signatures and material condition.

Measurements were conducted on two different types of ferrites which were then combined for the two-phase material study. Ferrites are ferrimagnetic ceramic compounds, derived from oxides of iron. They are generally used for high frequency applications such as inductors and transformers. This is because ferrites have high electrical resistance which leads to lower eddy current losses. Based on their crystallographic structure, ferrites are broadly classified into four categories: spinel, pervoskite, garnet and hexa ferrites.

The two ferrites studied are micron-sized spinel structured cobalt-manganese ferrite (soft ferrite) and nano-sized barium hexa-ferrite (hard ferrite). Spinel ferrites are magnetic iron oxides represented by a general formula AB_2O_4. Here A represents one of the metal ions (or a combination) with a valence state of two and B represents the metal ions with a valence state of three. Hexagonal ferrites (hexa ferrites) are magnetic iron oxides with a hexagonal structure. They are formed by iron, oxygen and one or more element that could be either barium, strontium, cobalt or a combination of these.

Barium hexaferrite ($BaFe_{12}O_{19}$ - hard phase) and cobalt manganese ferrite ($CoMn_{0.1}Fe_{1.9}O_4$ - soft phase), were ball-milled individually and then pressed into 1 inch, 0.5 inch and 0.25 inch pellets. This was followed by sintering at 1200 ^oC for 6 hours, in air atmosphere. The magnetic and microstructural properties of the single-phase material are discussed in the following sections.

4.2   Measurements and Analysis

Measurements and simulations were conducted to study the behavior and properties of the selected ferrites. The results from these studies are summarized in the following sections.

4.2.1   Microstructure analysis

The microstructure of the samples was analyzed using a FEI QUANTA field emission scanning electron microscope. Scanning electron microscopy (SEM) can be used to determine the microstructure and composition of samples. In SEM an image of the sample is produced by scanning it with a focused ion beam (FIB) of electrons. As the electron beams trace over the object, they interact with the surface of the object, dislodging secondary electrons from the surface of the specimen. A secondary electron detector is used to detect these electrons. Secondary electron images can reveal surface morphologies of the microstructure of a material. Similarly, backscattered electron sensors detect electrons that reflect off the surface of the specimen, typically known as backscattered electrons. These are more sensitive to compositional variations than the secondary electron images. Therefore contrasts in backscattered electron micrographs can be related to differences in composition in the microstructure of a material. The micrographs in this study were obtained in high vacuum mode at 15 kV and spot size of 3.5nm.

The SEM micrographs for cobalt manganese ferrite are seen in Fig. 4.1(a) and Fig.4.1(b) .
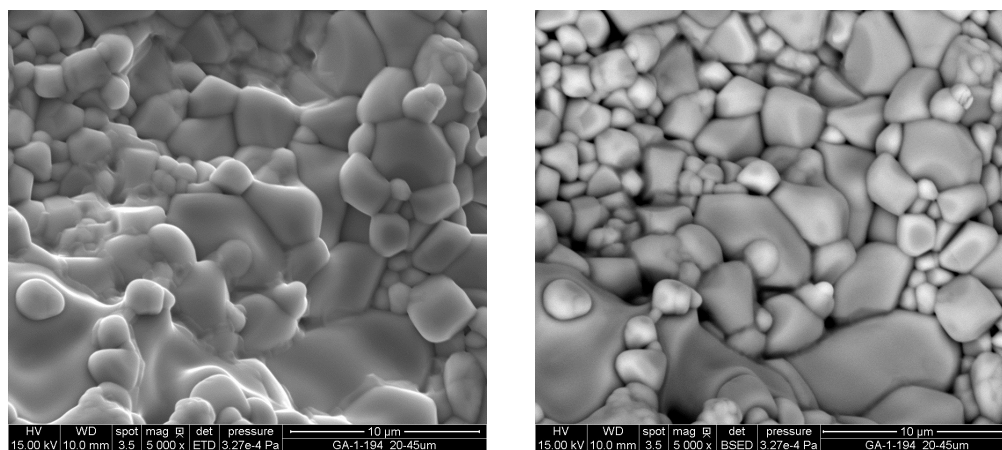
(a) Microstructure of Cobalt manganese-ferrite (Secondary emission pattern)

(b) Microstructure of Cobalt manganese-ferrite (Backscattered pattern)

Figure 4.1   Microstructure of cobalt-manganese ferrite

The SEM micrographs of barium hexaferrite formed by secondary and backscattered electrons are seen in Fig. 4.2(a) and Fig. 4.2(b). The geometric shape of the ferrite crystals is

(a) Microstructure of Barium hexaferrite (Secondary emission pattern)

(b) Microstructure of Barium hexaferrite (Backscattered pattern)
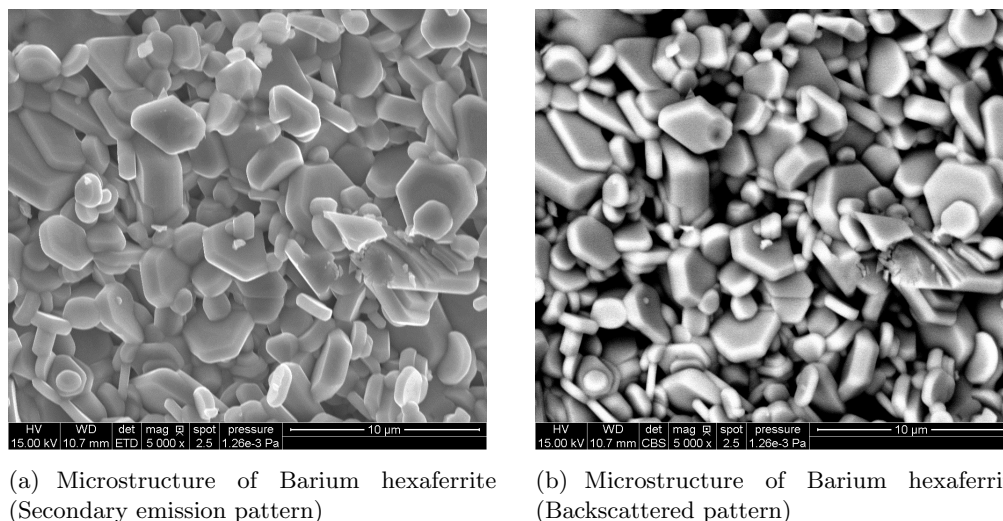
Figure 4.2   Microstructure of barium ferrite

clearly visible from the SEM micrographs.

4.2.2   Crystal structure analysis by X-ray diffractometry

The crystal structure of the samples was studied by X-ray diffractometry (XRD) using Cu K_α radiation at a wavelength of 0.154nm. The samples were scanned from from 10 degrees to 80 degrees at 45kV and 20mA.   The technique is based on the principle of X-ray diffraction governed by Bragg's law. The crystal atoms are arranged in a regular pattern. When the X-ray beam hits the crystal plane, constructive interference occurs in some directions and diffracted X-ray beams leave in varied directions. The diffracted beam comprises of several scattered rays from crystal planes mutually enforcing one another. The intensities of diffracted X rays for different angles (2 θ) give characteristic diffraction patterns as seen in Fig. 4.3(a) and Fig. 4.3(b). The corresponding peaks were indexed using XPert High Score Plus.

4.2.3   Magnetic measurements

The magnetic properties measurements for the single-phase samples were conducted using a hysteresis-graph measurement system at room temperature. The system uses an electromagnet to magnetize the test specimens. The specimens were placed between two electromagnets and the specimen completes the magnetic circuit. The samples were first demagnetized with
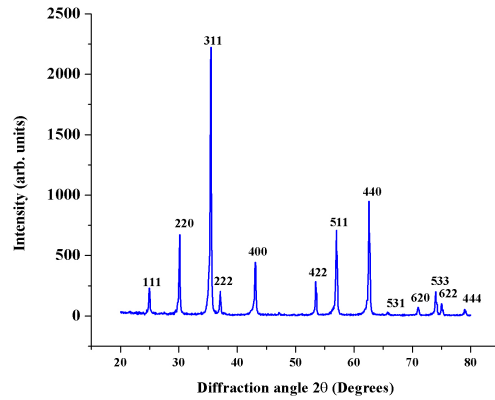
(a) XRD pattern for cobalt manganese ferrite
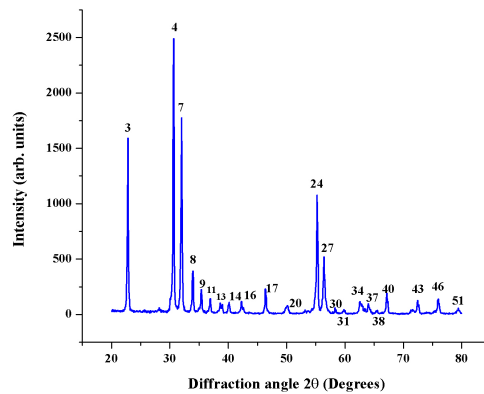
(b) XRD pattern for barium hexaferrite

Figure 4.3   X-ray diffraction patterns for single-phase ferrites

an AC magnetic field cycled between $\pm$ 1200 kA/m but with decreasing amplitude. During measurement, magnetic field up to 30000 A/m was applied with specimens placed between two poles of an electromagnet. A hall probe was used to measure the strength of the applied magnetic field H. The Hall voltage fluctuates in accordance with the strength of the magnetic field. Thus, the field strength can be determined by measuring the voltage. It is understood that the slope of the hysteresis curve or dM/dH indicates the differential susceptibility of the magnetic material. From the stochastic model of the Barkhausen effect we also know that the Barkhausen noise voltage is directly proportional to the differential susceptibility. A higher change in susceptibility would directly relate to an increase in Barkhausen activity.

The magnetic hysteresis characteristics of the individual ferromagnetic materials, barium hexaferrite and cobalt manganese ferrite can be seen in Fig.4.4(a) and Fig. 4.4(b) respectively. The saturation magnetization of the barium ferrite sample wasn't attained at maximum applied magnetic field of 30000 A/m. The cobalt ferrite sample attained saturation at a much lower value of magnetic field. The coercivity of the barium hexaferrite sample was 10000 A/m whereas the coercivity of the cobalt manganese-ferrite was one-tenth, 1000 A/m.

(a) Magnetic hysteresis in cobalt manganese ferrite

(b) Magnetic hysteresis in barium hexaferrite
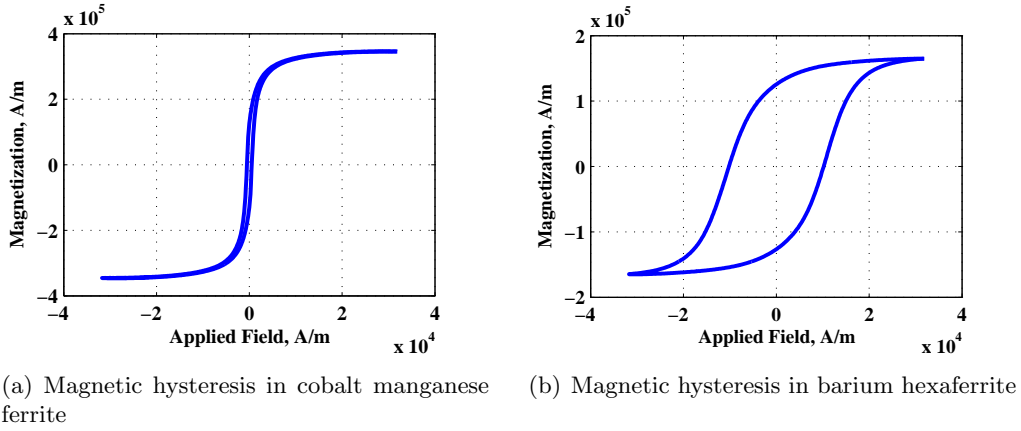
Figure 4.4   Magnetic hysteresis in ferrites

4.2.4   Barkhausen noise simulations

In order to simulate the Barkhausen noise profiles of the individual samples, first the Jiles-Atherton model parameters were obtained for each phase. The algorithm of choice is the deterministic sampling algorithm DIRECT (Divided Rectangles) [Finkel and Kelley (2006); Chwastek and Szczygowski (2007); Chwastek and Szczygłowski (2011); Raghunathan et al. (2012)]. The search for the global minimum is carried out by dividing the entire area into several hypercubes. The choice of data-points to be sampled is previously selected. This is defined by the bounds of the parameters to be extracted. The bounds selected for the operation of DIRECT are as indicated below.

1. Saturation Magnetization (M_s) lies between the bounds of M_{tip} and 1.2 M_{tip}.

2. Pinning Parameter k lies in(0.2 H_c, 5 H_c)

3. Reversibility c lies in (0,1)

4. Loop Shape Parameter a lies in $(0.5\ H_c, 5\ H_c)$

5. The domain coupling factor α can be assumed to be 0.7 H_{tip}/M_{tip}. It can be zero when there is no interaction between the magnetic moments.

6. Here H_{tip} is the value of field needed to saturate the modeled material and is assumed to be 10^4 A/m and M_{tip} is assumed to be equal to $1.547 * 10^6$ A/m.

The bounds for the J-A parameters can be varied to obtain an accurate fit based on the nature of the material. For example k the pinning parameter, which is also a measure of the coercivity of the material would vary for a hard and soft magnetic material. Similarly, the other bounds are material dependent.

The algorithm computes the J-A model parameters from the measured M-H data and recreates the hysteresis loop based on the estimated J-A parameters. The simulated M-H data was then used along-with the equations described in the stochastic model of the Barkhausen effect in equation 3.6 to simulate Barkhausen noise signals for each phase. The J-A model parameters for the individual measured phases are listed in Table. 4.1.

Table 4.1   Extracted Jiles-Atherton model parameters for individual measured phases

J-A Model Parameter	Soft Phase	Hard Phase
Reversibility Parameter	0.5	0.5
Pinning Parameter	1437.233	13326.036
Domain Density	1520.150	23064.293
Saturation Magnetization	3.801e+05	2.471e+05
Coupling factor	5.001e-03	2.902e-01

The simulated Barkhausen noise profiles from the measured hysteresis loops using these model parameters are plotted in Fig.4.5. Fig. 4.5(a) and Fig.4.5(b) respectively, show the Barkhausen noise profile obtained for the magnetically softer phase ($CoMn_{0.1}Fe_{1.9}O_4$) and the magnetically harder phase ($BaFe_{12}O_{19}$). This behavior can be modeled using the relation described in 3.6. For our simulations we assumed the initial number of Barkhausen events N to be 1000.

An alternative way of simulating the Barkhausen noise profiles is by directly using the measured magnetic hysteresis data and the equations from the stochastic model of the Barkhausen
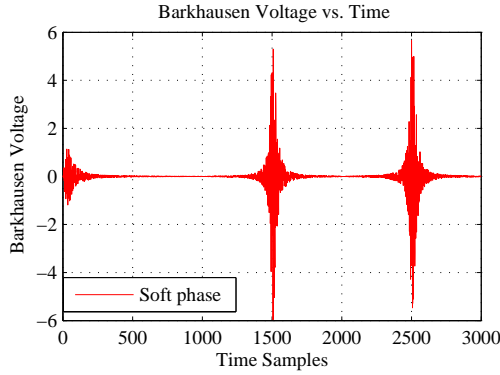
(a) Simulated Barkhausen noise profile for the cobalt manganese ferrite phase obtained from measured hysteresis loop using the J-A model parameters
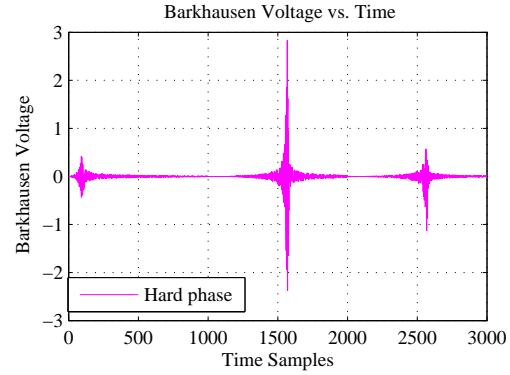
(b) Simulated Barkhausen noise profile for the barium hexaferrite phase obtained from measured hysteresis loop using the J-A model parameters

Figure 4.5   Simulated Barkhausen Noise profiles. In each figure the three peaks correspond to the initial magnetization, reverse magnetization cycle and forward magnetization cycle

effect. The values for dM/dH and dH/dt were computed from the measured data and the equations 3.4, 3.5 and 3.6 from the stochastic model of the Barkhausen effect were used to generate the stochastic variations. The simulations for the single-phase specimens are plotted in Fig. 4.6(a) and Fig. 4.6(b). Due to higher domain wall pinning, the coercivity of the barium hexaferrite is much higher than that of the cobalt ferrite. As a result, there would be less Barkhausen activity in the barium hexaferrite phase.
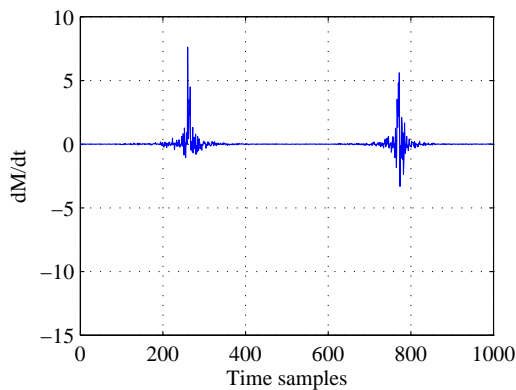
(a) Simulated Barkhausen noise profile for cobalt manganese ferrite
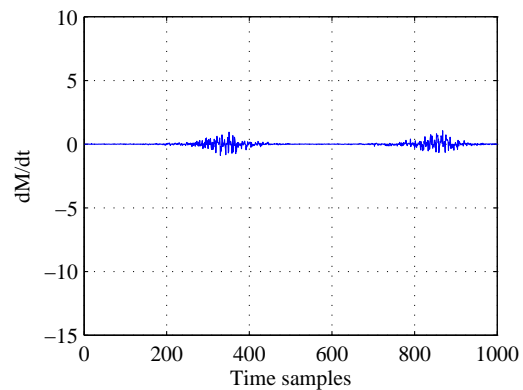
(b) Simulated Barkhausen noise profile for barium hexaferrite

Figure 4.6   Barkhausen noise profiles from simulation

4.2.5   Experimental verification of Barkhausen noise simulations

Before conducting room temperature Barkhausen noise measurements, the samples were thermally demagnetized. The Barkhausen noise signal was measured using a Rollscan 300 equipment designed by Stresstech and was controlled by the Microscan 600 software. The magnetizing frequency was selected to be 100 Hz and the filter was tuned to a range of $10 - 500$ kHz. The magnetizing voltage controls the magnitude of the magnetizing field applied to the sample. The sampling frequency was set to 2.5 MHz. This parameter determines the number of samples that are stored for signal analysis. The number of bursts was selected to be three. This parameter determines the magnetizing half cycles that will be stored for further signal analysis.
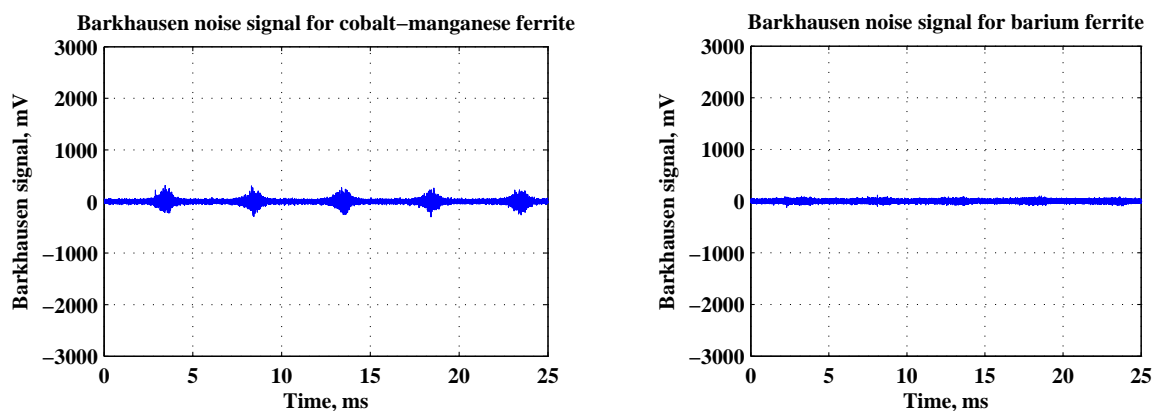
(a) Barkhausen noise profile for cobalt manganese ferrite   (b) Barkhausen noise profile for barium hexaferrite

Figure 4.7   Barkhausen noise profiles from measurements

Fig. 4.7(a) and Fig. 4.7(b) are the output Barkhausen noise voltage signals for a duration of 30 ms. The soft magnetic phase, for our study, $(CoMn_{0.1}Fe_{1.9}O_4)$, reaches saturation magnetization at a relatively lower applied field and can be easily magnetized and demagnetized. Meanwhile, hard magnetic materials, for this study, $(BaFe_{12}O_{19})$, has a higher resistance to demagnetization and a larger magnetic field needs to be applied opposite to the direction of applied field to reduce the magnetization of the sample to zero after reaching saturation magnetization. Thus, we observe pronounced Barkhausen activity for the softer magnetic phase in comparison to the harder magnetic phase.

From these measurements we can examine the microstructural and magnetic properties

of the single-phase magnetic materials, i.e. barium hexaferrite and cobalt manganese ferrite studied in this work. Due to the distinct differences in the magnetic behavior of each phase, we have selected these two materials as the constituents of a composite for further study on two-phase materials. The next chapter describes the two-phase material characterization in detail.

CHAPTER 5.   TWO-PHASE MATERIAL CHARACTERIZATION

5.1   Background

The results of study on two-phase composite material comprising of $(CoMn_{0.1}Fe_{1.9}O_4)$ and $(BaFe_{12}O_{19})$ are presented in this chapter. In magnetic hysteresis measurements, the interactions between constituent phases can be seen as a distortion in the hysteresis loop which depends on the volume fraction of the individual phases. An example of multiphase ferromagnetic composite can be found in materials which are finding applications in magnetic recording and data storage, magnetic sensors and actuators and exchange-spring magnets. Two-phase behavior can be achieved through deliberate engineering of the material, through addition of phases, thermal treatment which produces compositional variations and application of stress. Such behavior has been observed with changes in local strains, hardness and composition gradients in ferromagnetic steels [Blaow et al. (2004); Kinser (2005); Blaow et al. (2006); Raghunathan et al. (2012); Ktena et al. (2014)].

Fig. 5.1 shows hysteresis loops corresponding to a different magnetic phases. In this research $(CoMn_{0.1}Fe_{1.9}O_4)$ was used as the soft magnetic material (red curve), $(BaFe_{12}O_{19})$ served as the hard magnetic phase (magneta curve). The hysteresis loop of the combined phase was obtained by linear superposition (blue curve) and measured combined phase (black curve) indicates the measurement for the composite material.

Like magnetic hysteresis loops, Barkhausen noise (BN) emissions also represent changes in the magnetization behavior of a material when it is subjected to a continuously varying magnetic field [Kypris et al. (2013b)]. These emissions can be captured as voltage pulses using a sense coil placed in the vicinity of the test specimen. BN emissions are related to the interaction of the magnetic domains with the pinning sites during magnetization. Until now no model is
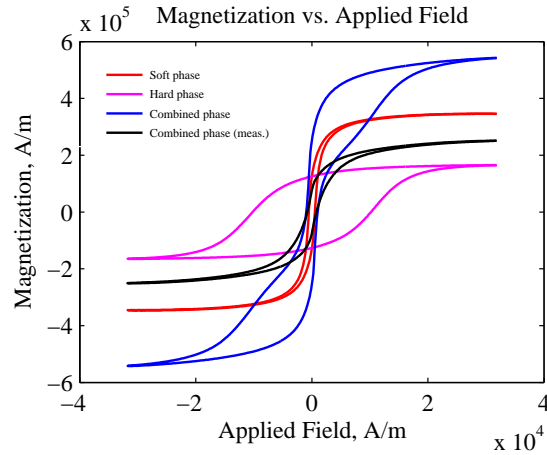
Figure 5.1   Hysteresis curves, a. Barium Hexaferrite ($BaFe_{12}O_{19}$) or hard phase (magneta curve), b. Cobalt-manganese ferrite ($CoMn_{0.1}Fe_{1.9}O_4$) or soft phase (red curve), c. Composition induced two-phase generated by linear addition of a and b (blue curve), d. Composition induced two-phase behavior (measured)

available which can be used to account for the distortions in the hysteresis behavior. Hence, several modifications have been made to the pre-existing models such as the Preisach model [Melikhov et al. (2000)]. Here, we introduce modifications to the Jiles-Atherton model to explain this phenomenon. Previous studies have extended the J-A model to incorporate anisotropy, magneto-elastic and thermal effects [Sablik and Jiles (1993); Wilson et al. (2002)]. Recently, it was extended to model the hysteresis of materials with two ferromagnetic phases [Raghunathan et al. (2012); Roy et al. (2012)]. In this chapter, the difference between Barkhausen noise emissions and hysteresis behavior for single phase and two-phase materials will be presented. It will also be shown that by making appropriate assumptions, both material properties can be modeled using Jiles-Atherton model.

5.2   Measurements and Analysis

A summary of the measurements conducted on the two-phase composite can be found in the following subsections. A standard ceramic sample preparation process was employed for producing these samples.

5.2.1 SEM and microstructure analysis

Microstructural analysis using the FEI Quanta system described in Chapter 4. Fig. 5.2(a), 5.2(b) shows the microstructure of barium hexaferrite ($BaFe_{12}O_{19}$), and cobalt manganese ferrite ($CoMn_{0.1}Fe_{1.9}O_4$). The grains are interspersed due to ball milling of the two powders together. No evidence of new phases was found in the micrographs.
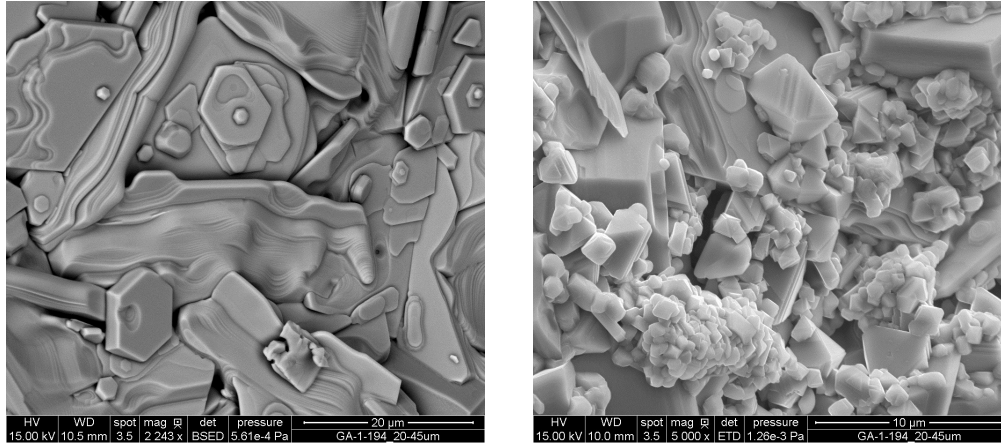
(a) Backscattered electron image of a region indicating greater concentration of the harder phase

(b) Secondary electron image of a region indicating a greater concentration of the softer phase

Figure 5.2   Microstructure of the ferrite composite

5.2.2 Crystallographic analysis by XRD

The X-ray diffraction pattern is shown in Fig. 5.3. Certain peaks observed at 2θ values not corresponding to those of the constituent ferrite angles are probably due to the formation of mixed phases after sintering the samples. However, examination of the microstructure on SEM did not reveal presence of a new phase with different morphology.

5.2.3 Magnetic measurements

The magnetic hysteresis loops obtained at room temperature using a hysteresisgraph measurement is shown in Fig. 5.4. Three hysteresis plots derived from the ($CoMn_{0.1}Fe_{1.9}O_4$), the ($BaFe_{12}O_{19}$) and a composite of both phases are shown. It can be seen that the hysteresis loop for the composite is a combination of the magnetic properties of the individual phases. There is
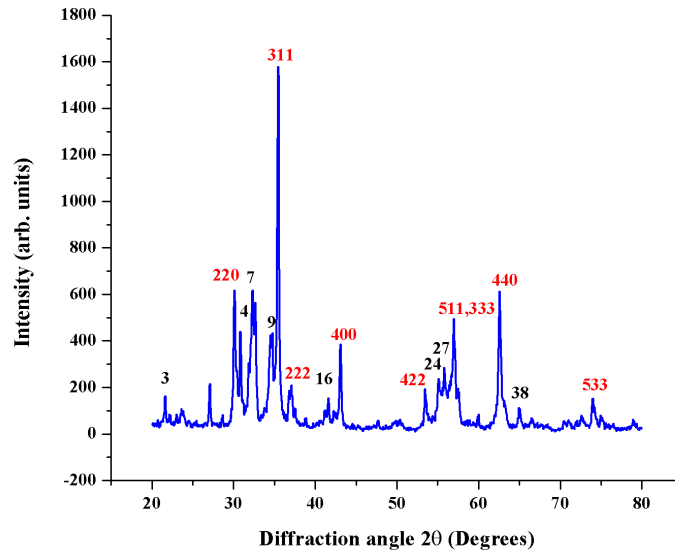
Figure 5.3   X-ray diffraction pattern of the composite comprising of cobalt-manganese ferrite
(red markers) and barium hexaferrite (black markers)

a decrease in the saturation magnetization in the two-phase composite when compared to the
hysteresis curves of the soft phase but an increase relative to the hard phase. The coercivity of
the composite is relatively closer to the coercivity of the cobalt manganese ferrite soft phase.
The decrease in both saturation magnetization and coercivity of the composite indicates that
the magnetic properties of the softer magnetic phase dominates.

5.2.4   Barkhausen noise simulations

In order to model the Barkhausen noise profiles for the two-phase magnetic materials such
as the one shown in Fig. 5.1, the J-A parameters for each individual phase were extracted
from the two-phase data. Using this set of parameters it is possible to reproduce the magnetic
hysteresis plot for each phase. For the two-phase material in Fig. 5.1, that will correspond to
a soft and a hard phase. This ability to use the J-A model to reconstruct the hysteresis curves
for individual phases and a combination of both phases in a composite based on the parameters
of the individual phases, offers the possibility of using the J-A model approach for developing
a NDE tool for composites with different magnetic phases.
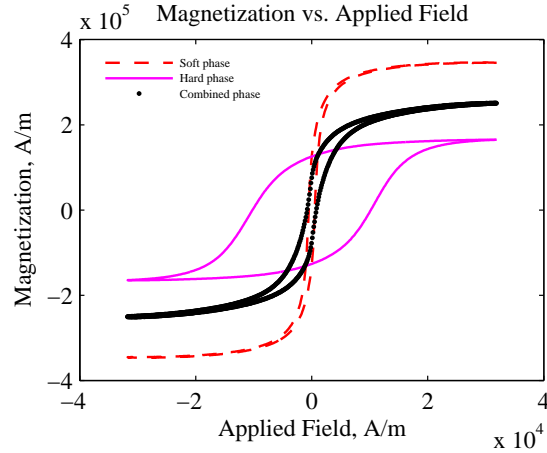
Figure 5.4   Hysteresis loops for the measured samples, a.   Cobalt-manganese ferrite ($CoMn_{0.1}Fe_{1.9}O_4$) or soft-phase (red), b. Barium hexaferrite ($BaFe_{12}O_{19}$) or hard phase (magenta), c. Combination of barium hexaferrite and cobalt-manganese ferrite (black)

In order to select appropriate J-A parameters for each phase, we used the optimization function which allows the estimation of the values of the J-A parameters by selecting a suitable range for each parameter [Finkel and Kelley (2006),Raghunathan et al. (2012)]. Table. 5.1 shows the J-A parameters for individual phases extracted from the magnetic hysteresis of barium hexaferrite-cobalt ferrite composite. With the exception of the pinning parameter, k, and domain density, a, the J-A parameters obtained are approximately in the expected range verified by comparing the values in Table. 4.1 and Table. 5.1. This deviation of the pinning parameter and domain density may be due to the coercivity of the soft phase dominating that of the hard phase, as seen in Fig. 5.4.

Table 5.1   Extracted Jiles-Atherton model parameters for combined measured phase

J-A Model Parameter	Soft Phase	Hard Phase
Reversibility Parameter c	0.5	0.5
Pinning Parameter k	1034.851	10348.515
Domain Density a	1411.161	13170.837
Saturation Magnetization M_s	2.759e+05	3.511e+05
Coupling factor α	6.351e-03	1.905e-01

Figures 5.5(a) and 5.5(b) correspond to the Barkhausen noise profiles for the simulated data which was obtained using the J-A model parameters for the soft and hard phase respectively.
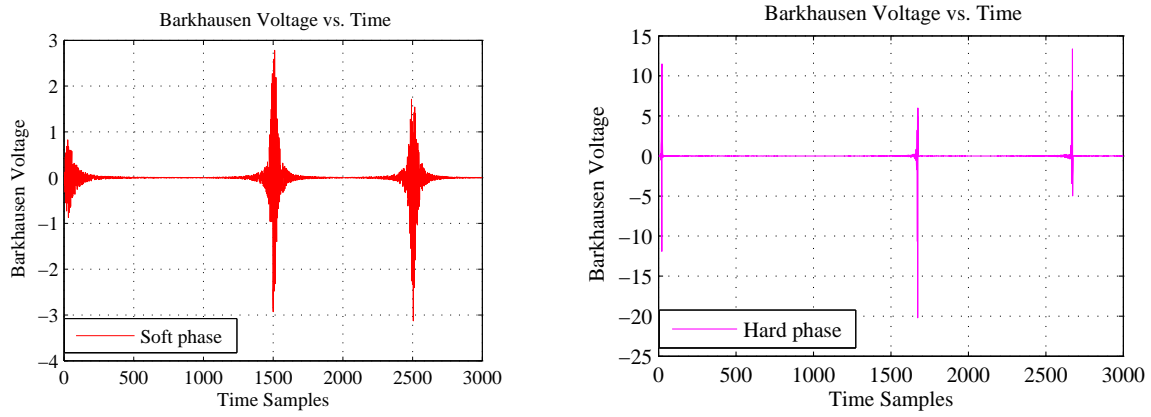
(a) BN profile for cobalt manganese ferrite in two-phase material obtained from the hysteresis loop reconstructed using the J-A model parameters

(b) BN profile for hard phase in two-phase material obtained from the hysteresis loop reconstructed using the J-A parameters

Figure 5.5   Barkhausen noise profiles. In each figure the three peaks correspond to the initial magnetization, reverse magnetization cycle and forward magnetization cycle

The simulations were also conducted using the measured M-H data along with the stochastic model equations 3.4, 3.5, 3.6. Since there is no sharp switching between the hard and soft magnetic phases, the stochastic Barkhausen noise generated through the simulation (Fig. 5.6(a)) doesn't indicate the presence of secondary peaks.

5.2.5   Experimental verification of Barkhausen noise simulations

MBE signals are strongly affected by microstructural changes because of the interactions between magnetic domains and microstructural features of the material. In Fig. 5.6 it is observed that the softer magnetic phase dominates the Barkhausen noise measurements. This may be because, in the hard magnetic phase, higher coercivity may be due to greater number of pinning sites, hence reduced domain wall movement and lesser contribution of the harder phase to Barkhausen activity as shown in Fig. 5.6(b).

5.3   Modeling of two-phase materials

In this study, an attempt was made to separate the contribution to the Barkhausen measurement by the constituent phases of the composite using the J-A model. We then characterized the hysteresis behavior using BN emission profiles.
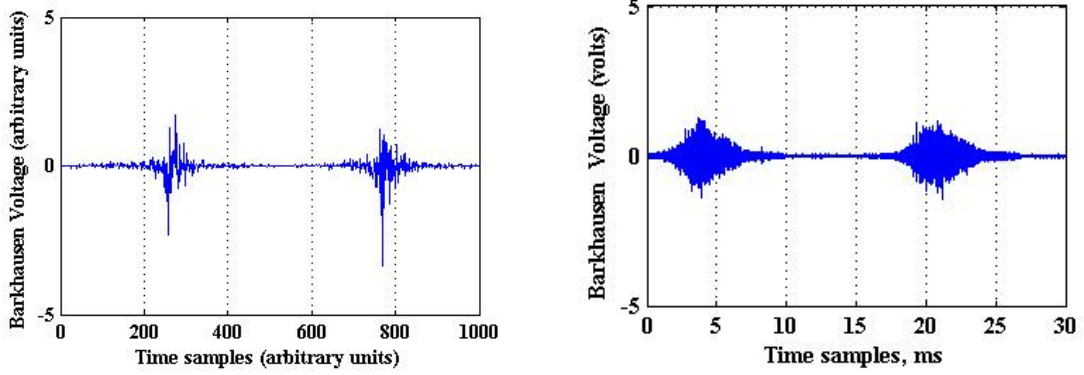
(a) Simulated Barkhausen noise profile of the composite

(b) Barkhausen noise profile of the composite

Figure 5.6   (a) Simulated Barkhausen noise profile for composite, (b) Measured Barkhausen noise profile for composite

A sharp switching in the magnetization loop, indicative of composite phases, may not necessarily be obtained. This may depend on the phase fraction of each material. In this work, an equal volume fraction of each phase was used. It is therefore essential to determine and model the volume fraction of either phase which would then help in understanding the contributions of each of the phases to the overall behavior. A scaling factor β was proposed to incorporate the effect of volume fraction of each phase. The peak intensity of the normalized Barkhausen voltage is related to the volume fraction of each phase. For our simulations, we assumed that each constituent phase had an equal volume fraction. Variation in the volume fractions would lead to an enhanced dominance of a particular phase and we could define 5.1 to include composition dependence using a scaling factor, β.

$$\frac{dM_{JS,total}}{dt} = \sum_{i=1}^{2} \frac{\beta(i)dM_{phase(i)}}{dt} \tag{5.1}$$

In order to understand the behavior of the composite, the simulated data for each phase were superposed. This operation is valid for the combined hysteresis curve that was obtained by linear addition of the individual phases, hence the Barkhausen noise signals can be linearly combined. This is equivalent to assuming no coupling between the two phases. Linear combination of Fig. 4.5(a) and 4.5(b) results in Fig. 5.7(a). Emergence of a secondary peak in the Barkhausen noise envelope is visible in this case. A similar operation on datasets from Fig.

5.5(a) and 5.5(b) resulted in Fig. 5.7(b). Both in Fig. 5.7(a) and Fig. 5.7(b) have two distinct peaks indicating the presence of two different ferromagnetic phases within the material. It can therefore be hypothesized that BN is sensitive to a composite comprising of two ferromagnetic phases. The bounds of the J-A parameters need to be selected appropriately such that the two-phases can be effectively separated out.
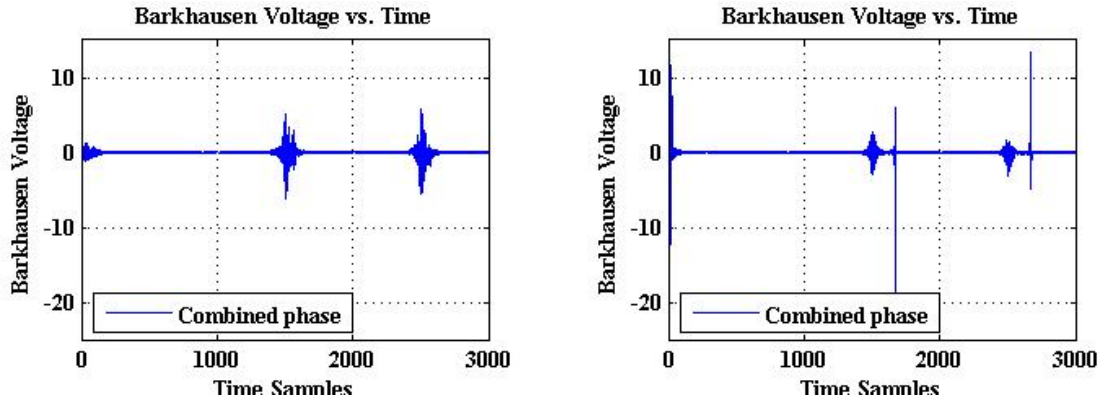
(a) Linear superposition of BN (4.5(a) and 4.5(b))   (b) Linear superposition of BN (5.5(a) and 5.5(b))

Figure 5.7   Summation of Barkhausen noise profiles

The observations reported in this section show that the magnetization in a composite material can be related to that of the constituent phases. Since we conduct linear superposition of the signals from the two individual phases we assume no coupling or interactions between the two phases. However, it can be said that the interaction between the constituent phases could be such that, depending on the volume fraction of phases, the contribution from one phase could dominate the magnetic properties obtained as the hysteresis loop and the Barkhausen noise signals. The inputs from the analysis presented above are used to propose modifications to the J-A model for describing the magnetization behavior of composites. Furthermore, 5.1 may be extended to more than two magnetic phases.

CHAPTER 6.   CONCLUSIONS

The two non-destructive evaluation techniques studied, namely, Barkhausen noise emission analysis and hysteresis measurements, can be used to characterize ferromagnetic phases within a magnetic material. Barkhausen emissions originate from within the magnetic domains in the material and can thus provide information on the variations in microstructure due to phase differences. Magnetic composite comprising of equal volumes of barium ferrite and cobalt manganese ferrite were studied. These two materials enabled the study of the Barkhausen noise profiles for a material with two different constituent phases. The conclusions derived from this study are listed below:

1. The analysis of the applicability of Jiles-Atherton model theory for two-phase materials has been examined for theoretically predicting the magnetic behavior of two phase materials with different individual magnetic characteristics. An extension for the model has been proposed along-with the stochastic model of the Barkhausen effect to take into account stochastic activity for each phase and extend the applicability of the approach to two phase materials. This has been achieved by introducing a linear summation in the relationship representing the stochastic model for the Barkhausen effect.

2. A stochastic model has been adopted to describe the Barkhausen noise profiles for single phase and two phase materials. It is demonstrated that simulation using this model shows two distinct peaks for linear summation of two distinct phases. It was attempted to verify the validity of this procedure for a typical composite consisting of two magnetic phases with equal volume fractions of each of the phases.

3. It has been demonstrated that the two techniques of the characterization of magnetic materials, the Barkhasuen noise analysis and magnetic hysteresis measurements, provide

complementary tools for nondestructive examination of magnetic materials. The magnetic hysteresis enables detection of the presence of multiple phases whereas Barkhausen noise analysis can provide information at microscopic scale such as presence of residual stresses, variations in microstructure or chemical composition variations, etc. under favorable situations. This can then be correlated to the magnetic hysteresis in order to better understand evolution of microstructural changes that affect magnetic materials.

4. The Barkhausen noise sensor has to have high sensitivity to detect signals from the constituent phases in multi-phase materials. Simulation of the working of a sensor for the detection and measurement of Barkhausen noise emissions were also conducted. It has been shown that the quality of observations depends on the design of the sensor. The main core parameters needed to optimize the performance of the sensor were identified to be: core geometry, core material, core length and core tip curvature.

6.1   Suggestions for future work

In this study, the two phases within a ferromagnetic composite were suitably separated into the individual phases by using the Jiles-Atherton Model and the DIRECT algorithm. Further characterization using stochastic model for Barkhausen effect was also conducted. The applicability of the present approach to characterize two phase materials with the help of J-A model may be extended to analyze multiphase materials enabling detection of phase constitution of materials and further quantitative determination of the volume fractions of each of the phases detected. The technique may be of particular interest to characterize multilayered films, microstructural evaluation of materials during service exposure, etc.

The simulation of performance of Barkhausen sensor should provide valuable inputs in designing probes with higher sensitivity especially adapted for targeted non-destructive evaluation such as detection of localized material properties, presence of anisotropy or compositional variations in materials. This can further help in designing sensors for capturing signals from greater depths in the materials under examination. The predictions made using the approach of simulation, however, needs further refinement particularly for miniaturization of the sensors.

APPENDIX A.   Presentations and Publications

A.1   Conference Presentations

1. ASNT Annual Conference, Charleston, South Carolina, 27-30 October 2014

2. IEEE Magnetics Summer School, Rio, Brazil, 9-16 August 2014.

3. IEEE International Magnetics Conference, Dresden, Germany, 4-8 May 2014.

4. CNDE I/U Sponsors Meeting, Ames, Iowa, 8 April 2014.

5. APS March Meeting, Denver, Colorado, 3-7 March 2014.

6. 58th Annual Magnetism and Magnetic Materials Conference, Denver, Colorado, 4-8 November 2013.

7. 10th International Conference on Barkhausen noise and Micromagnetic testing /QNDE, Baltimore, Maryland, 21-26 July 2013.

8. CNDE I/U Sponsors Meeting, Ames, Iowa, 8 April 2013.

9. APS March Meeting, Baltimore, Maryland, 18-22 March 2013.

A.2   Publications in Peer Reviewed journals

1. Analysis of Barkhausen noise emissions and magnetic hysteresis in multiphase magnetic materials, IEEE Transactions on Magnetics, Volume 50, Issue 11, (To be published in November 2014)

2. Optimization of sensor design for Barkhausen noise measurement using finite element analysis, Journal of Applied Physics 115, 17E512 (2014)

Optimization of sensor design for Barkhausen noise measurement using finite element analysis

N. Prabhu Gaunkar,[a] O. Kypris, I. C. Nlebedim, and D. C. Jiles
Department of Electrical and Computer Engineering, Iowa State University, Ames, Iowa 50011, USA

The effects of design parameters for optimizing the performance of sensors for magnetic Barkhausen emission measurement are presented. This study was performed using finite element analysis. The design parameters investigated include core material, core-tip curvature, core length, and pole spacing. Considering a combination of permeability and saturation magnetization, iron was selected as the core material among other materials investigated. Although a flat core-tip would result in higher magnetic flux concentration in the test specimen, a curved core-tip is preferred. The sensor-to-specimen coupling is thereby improved especially for materials with different surface geometries. Smaller pole spacing resulted in higher flux concentration. © 2014 AIP Publishing LLC. [http://dx.doi.org/10.1063/1.4864438]

I. INTRODUCTION

Barkhausen emissions occur due to sudden changes in magnetization within a ferromagnetic material and are obtained with application of a continuously varying magnetic field.[1] The emissions can be measured as induced voltage signals using induction sensors. Due to the strong interrelationship between the magnetic properties and microstructural features in ferromagnetic materials, Barkhausen effect presents a powerful tool for non-destructively monitoring the condition of such materials. This can be done by correlating the peak amplitude of the voltage pulse obtained during Barkhausen emission measurement with stress.[2,3] For industrial equipment, such monitoring of structural health is essential to avoid failures resulting from micro-structural changes, residual stresses, surface deformations, and microcracks generated in operations.

Apart from the stress-state or other micro-structural inhomogeneities in the materials, the detected Barkhausen signal also depends on the magnetizing field produced by the coils, the core geometry, sensor-to-specimen coupling, and spacing between core tips. It is therefore important that the sensor configuration be optimized to improve the sensitivity, reproducibility, and accuracy of the detected Barkhausen signals. In this study, it is shown how the choice of sensor design parameters affects the generation of magnetic fields used to excite Barkhausen emissions in a specimen. Using finite element simulations a method of optimizing these parameters for sensors with C-core geometries with two windings is demonstrated. The choice of performing DC simulations and thus ignoring frequency dependent effects is supported by the fact that typical Barkhausen noise excitation coils operate in the lower quasi-static limit and are thus well described by a DC approach.

II. THEORY

From Ampere's circuital law, for a magnetic circuit

$$\oint \mathbf{H} \cdot d\ell = NI. \qquad (1)$$

Here **H** is the magnetic field strength in the core, generated due to current I flowing in a coil having N turns. ℓ is the length of the flux path. The equivalent circuit of the magnetizing unit for this study is shown in Fig. 1(a). The total magnetic field strength due to the two magnetizing coils is taken to be 0.5 kA/m, in line with a previous study[4] on Barkhausen measurement. The two magnetizing coils can be approximated as solenoids of finite lengths. We can therefore find the field intensity along the axis, at a distance x from the center of the solenoid using the relation[5,6]

$$H = \frac{NI}{L} \left(\frac{L+2x}{2\sqrt{D^2 + (L+2x)^2}} + \frac{L-2x}{2\sqrt{D^2 + (L-2x)^2}} \right). \qquad (2)$$

D is the coil diameter, which for a C-core represents a coil with value shown in Table I. L is the length of the magnetizing coil. The magnetic field at the off-axis point C, which in this study is the center of the test specimen, is considered to be equivalent to the on-axis field at a distance x from the center of the coil. This is a valid approximation since the magnetic flux path is curved by the material, thus making it possible to set x = ABC. Therefore, we use this relationship to approximate the value of the magnetic field at the point marked C. Since the analytical expression is an approximation of the magnetic field at point C, we utilized finite element simulations for improved accuracy.

III. SIMULATION

Fig. 1(b) shows the geometry of the magnetizing unit. C-core geometry was selected, being a typical geometry for Barkhausen sensors. The number of turns and coil length for the magnetizing coils were calculated using Eq. (2). A DC magnetizing current of 1 A was assumed. The properties and dimensions of the core and the coil are listed in Table I. A finite element simulation was performed using the AC/DC module of COMSOL Multiphysics.

[a] Author to whom correspondence should be addressed. Electronic mail: neelampg@iastate.edu.
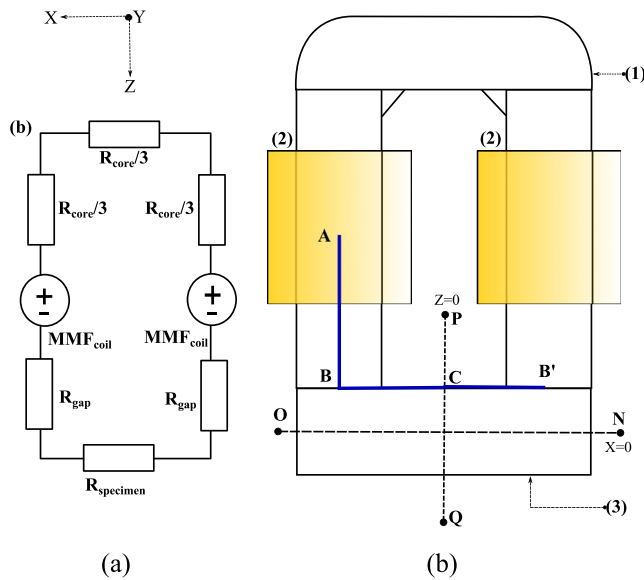
48

FIG. 1. (a) The equivalent magnetic circuit. (b) Schematic of the magnetizing assembly showing the core material (1), coils (2), and test specimen (3). Line segments NO and PQ represent sections along X and Z direction, respectively.

IV. RESULTS AND DISCUSSION

The effects of using different core materials for the magnetizing unit and the variations in the tip-curvature, length and inter-pole spacing of the core-materials have been investigated.

A. Effect of core material

Table II shows the core materials investigated including their electrical and magnetic properties. It can be seen in Fig. 2 that the maximum magnetic flux density in the material corresponds to the material with highest permeability. Although permalloy has the highest flux concentration, its

TABLE I. Core and coil dimensions (per pole).

Sensor	Coil	Core
Material	Copper	Variable
Length	8 mm	14 mm
Width	4 mm	3.4 mm
Depth	4 mm	3.4 mm
Number of Turns	32	N/A

TABLE II. Properties of the materials studied for use as the core material of the magnetizing unit.

Material	Electrical Conductivity S/m	Relative Permeability	Relative Permittivity
Air	0	1	1
Iron	1E7	5000 (Ref. 7)	300 (Ref. 8)
78 Permalloy	0.5E7	100000	5000 (Ref. 8)
Electrical Steel	2.12E6	4000	1
Ni-Zn Ferrite	2E-5 (Ref. 9)	1000 (Ref. 10)	14 (Ref. 9)
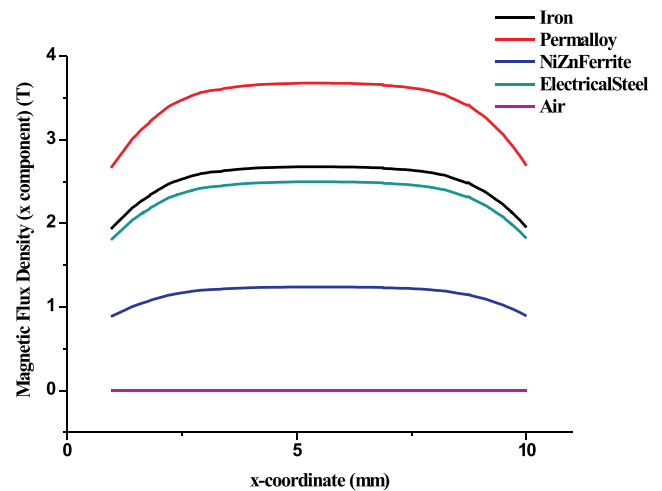
FIG. 2. Effect of material on magnetic flux density. Magnetic flux density was measured between the pole centers along the line segment NO as seen in Fig. 1(b).

saturation magnetization (0.86×10^6 A/m) is almost half of that of iron (1.71×10^6 A/m). Since it is important not to saturate the core material in application, iron was selected as the choice material for the rest of the study.

B. Effect of core-tip curvature

The effect of core-tip curvature on the magnetic flux density in the sample is shown in Fig. 3. The curvature of the core-tip is an important parameter to ensure good sensor-to-specimen coupling. Cores with flat, pointed and curved tips were investigated. Fig. 3 shows that the best performance can be obtained using a core-material with a flat tip. Nevertheless, in applications, a curved core-tip helps ensure consistent flux coupling with test specimens of varying surface geometries. Hence the core-tip curvature selected has an arc length of 3.45 mm that is slightly more than the length of a flat tip. Magnetic flux leakage occurs in the region between the core poles resulting in asymmetrical flux density above and below the test specimen.
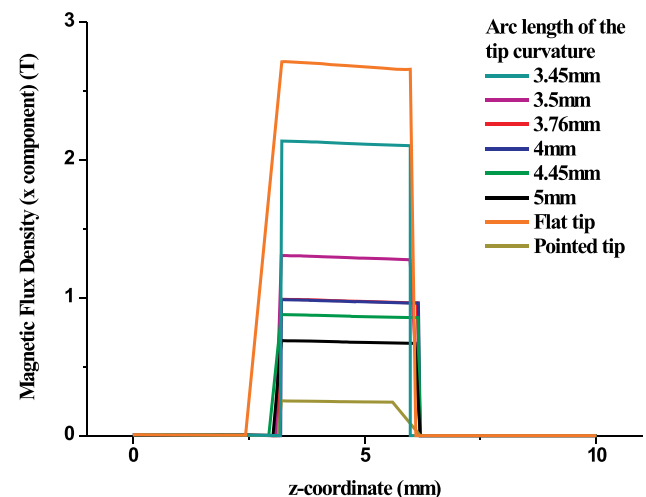

FIG. 3. Effect of tip curvature on the magnetic flux density. Magnetic flux density was measured along the line segment PQ as shown in Fig. 1(b).

17E512-3   Gaunkar *et al.*   J. Appl. Phys. **115**, 17E512 (2014)
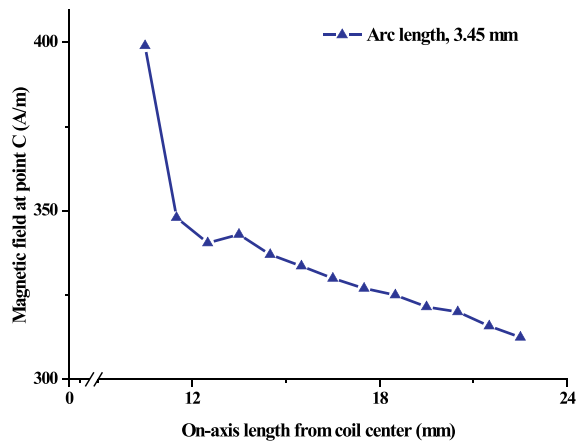
49

FIG. 4. Effect of core length on magnetic field. The on-axis length from coil center is defined as the length along path ABC, shown in Fig. 1(b). AB varies with increasing length of poles.
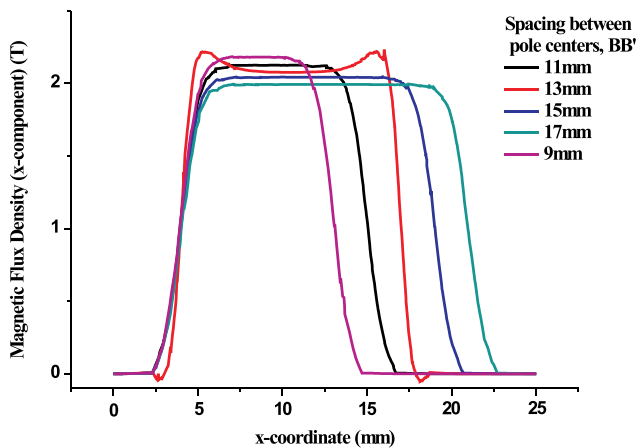

FIG. 5. Effect of pole spacing. The pole spacing was measured along the line segment NO, as shown in Fig. 1(b), where BB′ indicates the spacing between the pole centers.

C. Effect of core length

The effect of path length, ABC, of the core material on the generated magnetic field is shown in Fig. 4. These are obtained using an iron core with an arc length of 3.45 mm. The magnetic field strength decreases with increasing length of the core material. This is an important design consideration especially where varying the sensor size is necessary to test different parts of the same component. The maximum field strengths obtained at point C are in the range 0.31–0.4 kA/m. This is less than the 0.5 kA/m calculated and might be due to flux leakage. The maximum field penetration is obtained with the magnetizing coils are placed at a distance of 0.5 mm (i.e., closest to the test specimen). This was

incorporated into the design to observe the effect of spacing between the poles of the sensor.

D. Effect of inter-pole spacing

Fig. 5 shows the effect of varying the spacing between the two poles of the sensor. It can be seen that small spacing maximizes the magnetic flux density. In application, however, maximizing the flux density by decreasing the pole spacing should be balanced with the fact that measurement noise increases due to mutual inductance when the pole spacing is reduced. This is important considering that Barkhausen emissions are already noise-like.

V. CONCLUSIONS

The study carried out on the optimization of the sensor design parameters for Barkhausen emission measurements revealed the following. A sensor constructed with soft iron resulted in high magnetic field penetration into the test specimen. The sensor geometry governed the coupling between the sensor and the test specimen, a flat tip resulting in the best coupling. The sensor design can be further optimized to suit specific applications taking into consideration the parameters analyzed and described in this study.

[1] A. Dhar and D. Atherton, IEEE Trans. Magn. **28**, 3363 (1992).
[2] O. Kypris, I. C. Nlebedim, and D. C. Jiles, IEEE Trans. Magn. **48**, 4428 (2012).
[3] L. Mierczak, D. C. Jiles, and G. Fantoni, IEEE Trans. Magn. **47**, 459 (2011).
[4] O. Kypris, I. C. Nlebedim, and D. C. Jiles, IEEE Trans. Magn. **49**, 4148 (2013).
[5] D. C. Jiles, *Introduction to Magnetism and Magnetic Materials*, 1st ed. (Chapman and Hall, London and New York, 1991).
[6] A. E. Umenei, Y. Melikhov, and D. C. Jiles, IEEE Trans. Magn. **47**, 734 (2011).
[7] D. D. L. Chung, *Functional Materials: Electrical, Dielectric, Electromagnetic, Optical and Magnetic Applications (with Companion Solution Manual)*, Engineering Materials for Technological Needs Vol. 2 (World Scientific, Hackensack and New Jersey, London, 2010).
[8] J. S. Wilson, *Sensor Technology Handbook* (Elsevier, Amsterdam and Boston, 2005).
[9] A. Goldman, *Modern Ferrite Technology*, 2nd ed. (Springer, New York and NY, 2005).
[10] S. E. Lyshevski, *Nano- and Micro-Electromechanical Systems: Fundamentals of Nano- and Microengineering*, 2nd ed., Nano- and Microscience, Engineering, Technology, and Medicine Series Vol. 8 (CRC Press, Boca Raton [u.a.], 2005).

Analysis of Barkhausen noise emissions and magnetic hysteresis in multiphase magnetic materials

N. Prabhu Gaunkar[1], O. Kypris[1], I. C. Nlebedim[1], and D. C. Jiles[1], *Fellow, IEEE*

[1]Department of Electrical and Computer Engineering, Iowa State University, Ames, IA 50011 USA

Ferromagnetic materials can occur in single or multiphase and further more can undergo phase changes during processing or over time during service exposure. These phase changes can be attributed to physical processes or chemical reactions. In the present study we examine the hysteresis and Barkhausen emission profiles of two-phase magnetic materials. Besides magnetic hysteresis curves that can indicate the presence of more than one phase, we demonstrate that the Barkhausen noise signatures for two-phase materials form two-peaks in their Barkhausen voltage profile. This can be used as a tool for non-destructive evaluation of ferromagnetic materials employed in industrial applications.

Index Terms—**Hysteresis, Jiles-Atherton model, two-phase materials, multiphase materials, Barkhausen emission, non-destructive evaluation.**

I. INTRODUCTION

Hysteresis is the path dependent response of a material to an input based on its previous exposure to the input. It is commonly observed in ferromagnetic and ferroelectric materials when they are subjected to external magnetic and electric fields respectively. Several models [1]–[4] have been proposed to predict the hysteretic behavior of ferromagnetic materials. Of the available empirical models, the Preisach model [2] and the Jiles-Atherton (J-A) model [4] are widely used. In this study, we adopt the J-A model to study hysteresis in two-phase ferromagnetic materials.

The J-A model considers an array of distributed magnetic moments subjected to magnetic field, temperature and stress. The bulk magnetization of the material is obtained by integrating the distribution of magnetic moments over all the possible orientations. The changes in magnetization can then be subdivided into magnetic domain processes which contribute to reversible and irreversible changes in magnetization.

Besides magnetic hysteresis curves, magnetic Barkhausen effect (MBE) emissions also represent changes in the magnetization behavior of a material when it is subjected to a continuously varying magnetic field [5]. These emissions can be captured as voltage pulses using a sense coil placed in the vicinity of the test specimen. MBE emissions are related to the interaction of the magnetic domains with the pinning sites during magnetization [6].

Previous studies have extended the J-A model to incorporate anisotropy, magneto-elastic and thermal effects [7]–[9]. Recently, it has been extended to model the dynamic hysteresis of materials with two ferromagnetic phases [10]. In this study, we show that the MBE emission and hysteresis behavior for single phase and two-phase materials differ.

II. THEORY

A. Single phase and two-phase materials

Single phase magnetic materials usually exhibit a sigmoid shaped hysteresis curve over one cycle of applied magnetic field. In contrast, two (or multi) phase magnetic materials,

may exhibit distorted hysteresis curve, reflecting the presence of two or more magnetic phases in one hysteresis cycle. One of the phases switches at a lower coercive field and the other at a higher coercive field.
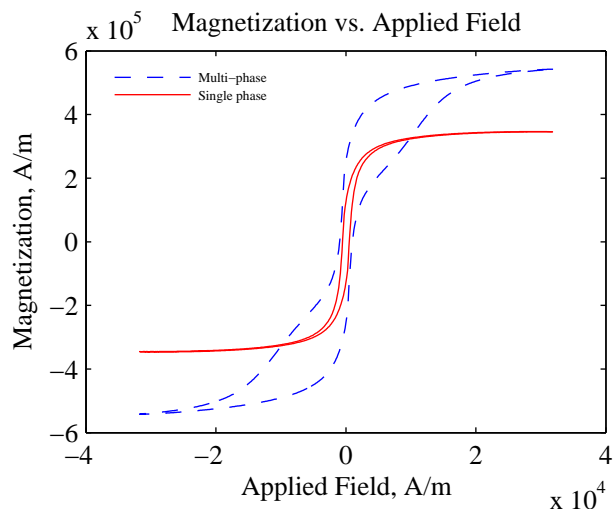
Fig. 1: Hysteresis curves for a single magnetic phase (red/solid) and a two-phase magnetic material (blue/dashed).

An example can be found in composite materials which are currently finding applications in magnetic sensors/ actuators, composite magneto-active materials and exchange-spring magnets. A second phase can form within a single phase matrix material as a result of external stress [11], changes in composition or sometimes by thermal processing. Fig.1 shows hysteresis loops corresponding to a single magnetic phase and a two-phase magnetic material. Whilst studies on models for single phase materials are extensive, there is still a need for a suitable model to properly represent the magnetic hysteresis in multi-phase magnetic materials. A suitable model will be able to predict the magnetic properties and performance of composite magnetic materials.

B. Jiles-Atherton Model

The J-A model was originally developed for describing the hysteresis behavior of a simple single-phase ferromagnetic material [4]. It uses five physical parameters; α, a, k, c and M_s to predict the magnetic hysteresis behavior of materials. α is the domain coupling coefficient, a is the domain density coefficient, k is the pinning coefficient, c is the reversibility coefficient and M_s is the saturation magnetization. The permeability is affected by domain coupling α, and domain density a. The pinning parameter k, is proportional to the density of pinning sites and the energy of pinning sites primarily determines the coercivity. The reversibility factor c, represents reversible domain wall bowing and rotation. Mathematically, the J-A model describes the hysteresis behavior of magnetic materials by solving the relation in (1) [4].

$$\frac{dM}{dH} = \frac{1}{(1+c)} \frac{M_{an} - M}{\delta k - \alpha(M_{an} - M)} + \frac{c}{(1+c)} \frac{dM_{an}}{dH} \quad (1)$$

Here H refers to the applied field and δ is a directionality parameter, ranging from +1 for the forward magnetization cycle, to -1 for the reverse magnetization cycle, M refers to the total magnetization, and M_{an} represents the anhysteretic magnetization. M can be further subdivided into the irreversible (M_{irr}) and reversible magnetization (M_{rev}) as in (2).

$$M = M_{irr} + M_{rev} \quad (2)$$

The reversible magnetization is attributed to domain wall bowing, reversible translation and reversible rotation whereas the irreversible magnetization is primarily due to domain wall pinning and irreversible rotation. The anhysteretic magnetization can be described using the Langevin function as described in (3). This relation highlights the dependence of M_{an} on the saturation magnetization M_s, the domain density, a and the effective applied field H_e.

$$M_{an} = M_s \left(\coth \frac{H_e}{a} - \frac{a}{H_e} \right) \quad (3)$$

The effective field is considered to be a combination of the applied field H and the magnetization M scaled by the coupling parameter α as follows

$$H_e = H + \alpha M \quad (4)$$

In order to model the hysteresis behavior in two phase materials as shown in Fig.1, the J-A parameters for each phase are extracted. Using this set of parameters we reproduce the magnetic hysteresis plot for each phase. For a two-phase material, for example, with a hard and soft phase that are not coupled as shown in Fig.1, the two sets of parameters should yield hysteresis loops corresponding to those separate magnetically hard and soft phases. This ability to reproduce the hysteresis plots of constituent phases of a composite or a combined hysteresis plot of the phases present using the plots of the J-A model, presents a viable approach for non-destructive evaluation of the two phase materials.

C. Stochastic Model for Barkhausen effect

The stochastic nature of the Barkhausen emissions have been studied in detail [12]–[14]. Although Barkhausen emissions result from discontinuous magnetization changes inside

a material, they can be measured on the surface of the material using an inductive sensor. We use this interesting feature of MBE emission and correlate it to the magnetization to study the ferromagnetic phases within the material. From Faraday's law of electromagnetic induction the induced emf, V_{emf}, sensed by the Barkhausen sensor is proportional to the rate of change of magnetic flux with time $d\phi/dt$ which is equivalent to the rate of change of magnetization with time scaled by the area of the pick-up coil and the permeability of free space. Alternatively, the sum of the magnetization jumps (jump sum magnetization dM_{JS}/dt) due to the irreversible component of magnetization is related to Barkhausen emissions. The relationship between the induced emf, the time rate of change of M_{JS} and the irreversible magnetization component due to an applied magnetic field is shown in (5) where dM_{irr}/dH is the differential susceptibility and dH/dt is the time rate of change of the applied magnetic field [15], [16].

$$|V_{emf}| \propto \frac{dM_{JS}}{dt} = \gamma \frac{dM_{irr}}{dH} \frac{dH}{dt} \quad (5)$$

Here γ represents the ratio of the discontinuous magnetization M_{disc} to the irreversible component of magnetization M_{irr} multiplied by N_t, the number of Barkhausen events occurring in a given time period. $\langle M_{disc} \rangle$ represents average discontinuous change in magnetization. In this case it is considered to be an ensemble average. It is also a very small quantity. Numerically,

$$\gamma = \frac{d\langle M_{disc} \rangle N_t}{dM_{irr}} = \langle M_{disc} \rangle \frac{dN_t}{dM_{irr}} + N_t \frac{d\langle M_{disc} \rangle}{dM_{irr}} \quad (6)$$

It was found that the size of the Barkhuasen jumps is considered to be weakly related to the irreversible change in magnetization and thus, γ can be approximated to be equal to $\langle M_{disc} \rangle dN_t/dM_{irr}$. The random nature of Barkhausen emissions allows the number of events, N_t, to be described by a recursive relation wherein the number of events is always held to be a positive, non-zero quantity. The increment in the number of events with time is assumed to follow a Poisson distribution [14]. The number of events, N_t in the time interval t, is related to the number of events N_{t-1} in the previous time interval $t-1$ as seen in (7).

$$N_t = N_{t-1} + \delta_{rand}\sqrt{N_{t-1}}; \quad (7)$$

δ_{rand} is a random number lying in the range $\pm$ 1.47. Originally, δ_{rand} was assumed to lie in the range $\pm$ 1. However 32 % of the time the increment in N_t should be beyond one standard deviation [14]. Incorporating equations (5), (6) and (7) we model the Barkhausen activity as described by the relation in (8) [14].

$$\frac{dM_{JS}}{dt} = \frac{dM_{irr}}{dH} \frac{dH}{dt} \langle M_{disc} \rangle \frac{dN_t}{dM_{irr}} \quad (8)$$

Equation (8) shows that the magnetization jump sum is proportional to the number of Barkhausen activities resulting from discontinuous magnetization process. Equations (1) and (8) form the foundation for the stochastic-hysteretic model for Barkhausen emissions. In the following sections we extend these relations to describe the Barkhausen noise signals in two-phase magnetic materials.

III. Experimental Details

Constituent powders, barium hexaferrite ($BaFe_{12}O_{19}$ - hard phase) and cobalt manganese ferrite ($CoMn_{0.1}Fe_{1.9}O_4$ - soft phase), were first ball-milled and then pressed into 1 inch, 0.5 inch and 0.25 inch pellets. This was followed by sintering at a temperature of 1200 ^oC for a duration of 6 hours, in air atmosphere. Individual samples of each phase were also prepared. The magnetic hysteresis measurements on the samples were carried out using a hysteresis-graph measurement system.

In order to select appropriate J-A parameters for each phase, we used the optimization function in [10], [17]. This function allows the estimation of the values of the J-A parameters by selecting a suitable range for each parameter. Table. I shows the J-A parameters for two-phase behavior contributed to the composite magnetic hysteresis by the individual phases. A similar procedure was carried out for the barium hexaferrite-cobalt ferrite composite. Table. II shows the J-A parameters for this composition. With the exception of the pinning parameter, k, and domain density, a, the J-A parameters obtained are approximately in the expected range verified by comparing the values in Table. I and Table. II.

TABLE I: Extracted Jiles-Atherton model parameters for individual measured phases

J-A parameters	Soft Phase	Hard Phase
Reversibility Parameter, c	0.5	0.5
Pinning Parameter, k	1437.233	13326.036
Domain Density, a	1520.150	23064.293
Saturation Magnetization, Ms	3.801e+05	2.471e+05
Coupling factor, α	5.001e-03	2.902e-01

TABLE II: Extracted Jiles-Atherton model parameters for combined measured phase

J-A parameters	Soft Phase	Hard Phase
Reversibility Parameter, c	0.5	0.5
Pinning Parameter, k	1034.851	10348.515
Domain Density, a	1411.161	13170.837
Saturation Magnetization, Ms	2.759e+05	3.511e+05
Coupling factor, α	6.351e-03	1.905e-01

IV. Results and Discussion

Fig. 2 shows the microstructure of the two-phase material used in this work which comprises of barium hexaferrite ($BaFe_{12}O_{19}$), a harder magnetic material and cobalt manganese ferrite ($CoMn_{0.1}Fe_{1.9}O_4$), a softer phase. A standard ceramic sample preparation process was employed for producing these samples.

Fig. 3 shows three hysteresis plots derived from the $CoMn_{0.1}Fe_{1.9}O_4$ phase, the $BaFe_{12}O_{19}$ phase and a composite of both phases. It can be seen that the hysteresis loop for the composite is different from that derived from individual phases which indicates magnetic coupling between the two phases in the composite. In this study, we have attempted to separate the constituent phases of the two-phase material by using the J-A model and the five physical model parameters. We then characterized the hysteresis behavior using MBE emission profiles.

The stochastic model of the Barkhausen effect, as formulated in (8) was utilized to observe the Barkhausen noise profile of the individual phases. For our simulations we
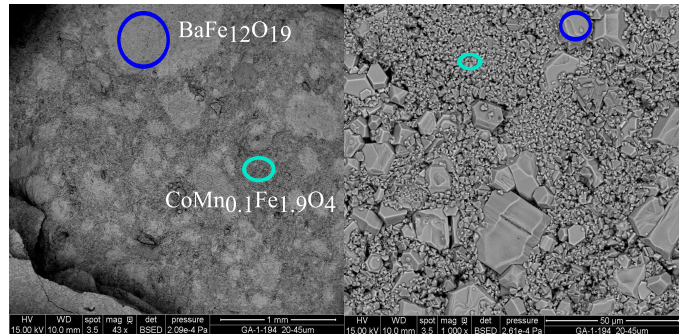

Fig. 2: Microstructure of the two-phase composite sample. White regions correspond to barium hexaferrite whereas dark regions correspond to cobalt manganese ferrite (left figure). Microstructure at higher magnification higlighting the two different regions (right figure).
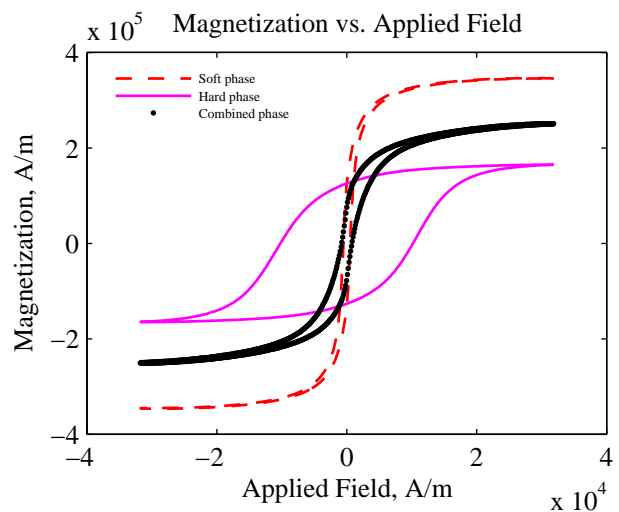

Fig. 3: Hysteresis loops for the measured samples for cobalt-manganese ferrite ($CoMn_{0.1}Fe_{1.9}O_4$) or soft-phase (red/dashed). Barium hexaferrite ($BaFe_{12}O_{19}$) or hard phase (magenta/solid). Combination of barium hexaferrite and cobalt-manganese ferrite(black/dotted).

assumed the initial number of Barkhausen events, N_t, to be 1000. Fig. 4(a) shows the MBE profile obtained for the magnetically softer phase ($CoMn_{0.1}Fe_{1.9}O_4$) followed by that of the magnetically harder phase ($BaFe_{12}O_{19}$) in Fig. 4(b). This behavior can be modeled using the relation described in (9).

$$\frac{dM_{JS,total}}{dt} = \beta_1 \frac{dM_{phase1}}{dt} + \beta_2 \frac{dM_{phase2}}{dt} \qquad (9)$$

Here β indicates the volume fraction.

Since addition of the hysteresis components for individual phases was obtained by linear combination, summation of the MBE was carried out. This operation results in a MBE profile with emergence of secondary peaks as seen in Fig. 4(e). A similar operation was also carried out for the constituent phases. Fig. 4(c) shows the MBE profile for the softer phase that was identified using the J-A model. Fig. 4(d) shows the MBE profile for the harder phase that was identified. The linear superposition of the MBE profiles, Fig. 4(c) and Fig. 4(d), leads to Fig. 4(f). Both in Fig. 4(e) and Fig. 4(f)

we observe two distinct peaks which indicates the presence of two different ferromagnetic phases within the material. These observations lead to the conclusion that the magnetic behavior of two (or multi) phase composite materials can be characterized from the MBE profiles. To do this the bounds of the J-A parameters need to be selected appropriately such that the two-phases can be effectively separated out. Similar behavior has been observed with changes in local strains, hardness and composition gradients in ferromagnetic steels [11], [18], [19]. The peak intensity of the normalized Barkhausen voltage is related to the volume fraction of each phase. For our simulations, we assumed that each phase had an equal volume fraction i.e. β is equal to 1. Variations in the volume fractions would lead to the reflection of an enhanced or diminished response corresponding to the particular phases. We could further define (9) to include dependence on composition variations, for example, using a scaling factor, β.
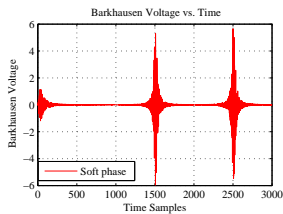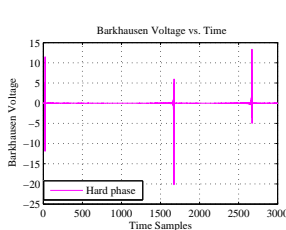

(a) BN profile for the soft phase obtained from measured hysteresis loop using the J-A model parameters
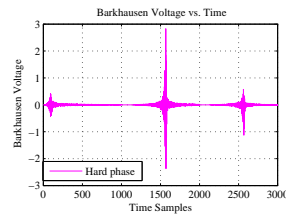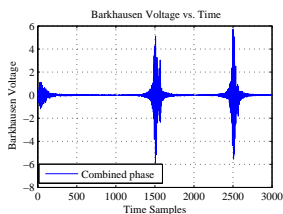
(b) BN profile for the hard phase obtained from measured hysteresis loop using the J-A model parameters
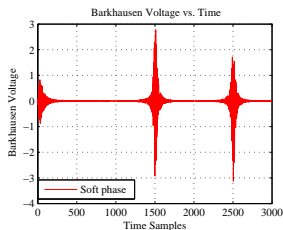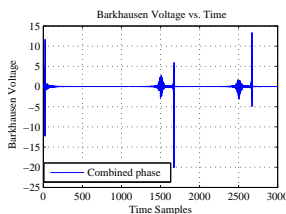
(c) BN profile for soft phase in two-phase material obtained from the hysteresis loop reconstructed using the J-A model parameters

(d) BN profile for hard phase in two-phase material obtained from the hysteresis loop reconstructed using the J-A parameters

(e) Linear superposition of BN (a and b)

(f) Linear superposition of BN (c and d)

Fig. 4: Barkhausen Noise profiles. In each figure the three voltage bursts correspond to the initial magnetization, reverse magnetization cycle and forward magnetization cycle.

V. Conclusions

This study shows that the Jiles-Atherton theory can be extended to describe the magnetic behavior of two phase ferromagnetic materials. The J-A model has been applied to analyze the magnetic behavior of the magnetic phases of a two phase

material. The stochastic-hysteretic model for the Barkhausen effect allowed us to describe the Barkhausen noise profile for single-phase and two-phase materials. The two distinct peaks were observed for composites, as in the present study comprising of equal proportions of each magnetic phase. The model can be utilized as a tool for non destructive evaluation of two phase ferromagnetic materials for the detection and characterization of constituent phases.

References

[1] L. L. E. Landau, "On the theory of the dispersion of magnetic permeability in ferromagnetic bodies," in *Physik. Z. Sowjetunion*, 1935, vol. 8, pp. 153–169.

[2] F. Preisach, "Über die magnetische Nachwirkung," *Zeitschrift für Physik*, vol. 94, no. 5-6, pp. 277–302, 1935.

[3] E. W. E. Stoner, "A mechanism of magnetic hysteresis in heterogeneous alloys," in *Philosphical Transactions of the Royal Society of London*, 1948, pp. 599–642.

[4] D. Jiles and D. Atherton, "Theory of ferromagnetic hysteresis," *Journal of Magnetism and Magnetic Materials*, vol. 61, no. 1-2, pp. 48–60, 1986.

[5] O. Kypris, I. C. Nlebedim, and D. C. Jiles, "Experimental verification of the linear relationship between stress and the reciprocal of the peak barkhausen voltage in astm a36 steel," *IEEE Transactions on Magnetics*, vol. 49, no. 7, pp. 4148–4151, 2013.

[6] M. Dimian and P. Andrei, *Noise-driven phenomena in hysteretic systems*, ser. Signals and communication technology. Springer, 2014, vol. 218.

[7] K. Chwastek and J. Szczygłowski, "The effect of anisotropy in the modified Jiles-Atherton model of static hysteresis," *Archives of Electrical Engineering*, vol. 60, no. 1, 2011.

[8] M. Sablik and D. Jiles, "Coupled magnetoelastic theory of magnetic and magnetostrictive hysteresis," *IEEE Transactions on Magnetics*, vol. 29, no. 4, pp. 2113–2123, 1993.

[9] P. Wilson, J. Ross, and A. Brown, "Simulation of magnetic component models in electric circuits including dynamic thermal effects," *IEEE Transactions on Power Electronics*, vol. 17, no. 1, pp. 55–65, 2002.

[10] A. Raghunathan, Y. Melikhov, J. Snyder, and D. Jiles, "Modeling of two-phase magnetic materials based on Jiles–Atherton theory of hysteresis," *Journal of Magnetism and Magnetic Materials*, vol. 324, no. 1, pp. 20–22, 2012.

[11] A. Raghunathan, P. Klimczyk, and Y. Melikhov, "Application of Jiles-Atherton Model to Stress Induced Magnetic Two-Phase Hysteresis," *IEEE Transactions on Magnetics*, vol. 49, no. 7, pp. 3187–3190, 2013.

[12] B. Alessandro, C. Beatrice, G. Bertotti, and A. Montorsi, "Domain-wall dynamics and Barkhausen effect in metallic ferromagnetic materials. I. Theory," *Journal of Applied Physics*, vol. 68, no. 6, p. 2901, 1990.

[13] G. Bertotti and I. D. Mayergoyz, *The Science of Hysteresis*. Amsterdam and Boston: Academic Press, 2006.

[14] D. C. Jiles, "Dynamics of domain magnetization and the Barkhausen effect," *Czechoslovak Journal of Physics*, vol. 50, no. 8, pp. 893–924, 2000.

[15] A. Mitra and D. Jiles, "Effects of tensile stress on the magnetic Barkhausen effect in 2605 CO amorphous alloy," *IEEE Transactions on Magnetics*, vol. 31, no. 6, pp. 4020–4022, 1995.

[16] D. C. Jiles, L. B. Sipahi, and G. Williams, "Modeling of micromagnetic Barkhausen activity using a stochastic process extension to the theory of hysteresis," *Journal of Applied Physics*, vol. 73, no. 10, p. 5830, 1993.

[17] D. E. Finkel and C. T. Kelley, "Additive Scaling and the DIRECT Algorithm," *Journal of Global Optimization*, vol. 36, no. 4, pp. 597–608, 2006.

[18] A. Ktena, E. Hristoforou, G. J. Gerhardt, F. P. Missell, F. J. Landgraf, D. L. Rodrigues, and M. Alberteris-Campos, "Barkhausen noise as a microstructure characterization tool," *Physica B: Condensed Matter*, vol. 435, pp. 109–112, 2014.

[19] M. Blaow, J. Evans, and B. Shaw, "Effect of hardness and composition gradients on Barkhausen emission in case hardened steel," *Journal of Magnetism and Magnetic Materials*, vol. 303, no. 1, pp. 153–159, 2006.

BIBLIOGRAPHY

Alessandro, B., Beatrice, C., Bertotti, G., and Montorsi, A. (1990). Domain-wall dynamics and Barkhausen effect in metallic ferromagnetic materials. I. Theory. *Journal of Applied Physics*, 68(6):2901.

Bertotti, G. (1983). Space-time correlation properties of the magnetization process and eddy current losses: Theory. *Journal of applied physics*, 54(9):5293–5305.

Bertotti, G. (1998). *Hysteresis in magnetism: For physicists, materials scientists, and engineers.* Electromagnetism. Academic Press, San Diego.

Bertotti, G. and Mayergoyz, I. D. (2006). *The Science of Hysteresis.* Academic Press, Amsterdam and Boston.

Blaow, M., Evans, J., and Shaw, B. (2004). Effect of deformation in bending on magnetic Barkhausen noise in low alloy steel. *Materials Science and Engineering: A*, 386(1-2):74–80.

Blaow, M., Evans, J., and Shaw, B. (2006). Effect of hardness and composition gradients on Barkhausen emission in case hardened steel. *Journal of Magnetism and Magnetic Materials*, 303(1):153–159.

Chung, D. D. L. (2010). *Functional materials: Electrical, dielectric, electromagnetic, optical and magnetic applications (with companion solution manual) / Deborah D.L. Chung*, volume 2 of *Engineering materials for technological needs*. World Scientific, Hackensack and N.J. and London.

Chwastek, K. and Szczygłowski, J. (2011). The effect of anisotropy in the modified Jiles-Atherton model of static hysteresis. *Archives of Electrical Engineering*, 60(1).

Chwastek, K. and Szczygowski, J. (2007). An alternative method to estimate the parameters of jilesatherton model. *Journal of Magnetism and Magnetic Materials*, 314(1):47 – 51.

Dimian, M. and Andrei, P. (2014). *Noise-driven phenomena in hysteretic systems*, volume 218 of *Signals and communication technology*. Springer.

Finkel, D. E. and Kelley, C. T. (2006). Additive Scaling and the DIRECT Algorithm. *Journal of Global Optimization*, 36(4):597–608.

Gaunkar, N. P., Kypris, O., Nlebedim, I., and Jiles, D. (2014). Optimization of sensor design for barkhausen noise measurement using finite element analysis. *Journal of Applied Physics*, 115(17):17E512.

Goldman, A. (2005). *Modern ferrite technology*. Springer, New York and NY, 2 edition.

Jiles, D. (1988). Review of magnetic methods for nondestructive evaluation. *NDT International*, 21(5):311–319.

Jiles, D. (1998). *Introduction to magnetism and magnetic materials*. Chapman and Hall, London and New York, 2 edition.

Jiles, D. and Atherton, D. (1986). Theory of ferromagnetic hysteresis. *Journal of Magnetism and Magnetic Materials*, 61(1-2):48–60.

Jiles, D. C. (2000). Dynamics of domain magnetization and the Barkhausen effect. *Czechoslovak Journal of Physics*, 50(8):893–924.

Jiles, D. C., Sipahi, L. B., and Williams, G. (1993). Modeling of micromagnetic Barkhausen activity using a stochastic process extension to the theory of hysteresis. *Journal of Applied Physics*, 73(10):5830.

Kaplan, M., Gür, C. H., and Erdogan, M. (2007). Characterization of Dual-Phase Steels Using Magnetic Barkhausen Noise Technique. *Journal of Nondestructive Evaluation*, 26(2-4):79–87.

Kinser, E. (2005). Magnetic nondestructive characterization of case depth in surface-hardened steel. Master's thesis, Iowa State University, Ames, Iowa.

Ktena, A., Hristoforou, E., Gerhardt, G. J., Missell, F. P., Landgraf, F. J., Rodrigues, D. L., and Alberteris-Campos, M. (2014). Barkhausen noise as a microstructure characterization tool. *Physica B: Condensed Matter*, 435:109–112.

Kypris, O., Nlebedim, I. C., and Jiles, D. C. (2012). Mapping Stress as a Function of Depth at the Surface of Steel Structures Using a Frequency Dependent Magnetic Barkhausen Noise Technique. *IEEE Transactions on Magnetics*, 48(11):4428–4431.

Kypris, O., Nlebedim, I. C., and Jiles, D. C. (2013a). A New Method for Obtaining Stress-Depth Calibration Profiles for Non-Destructive Evaluation Using a Frequency-Dependent Model of Barkhausen Emissions. *IEEE Transactions on Magnetics*, 49(7):3893–3896.

Kypris, O., Nlebedim, I. C., and Jiles, D. C. (2013b). Experimental verification of the linear relationship between stress and the reciprocal of the peak barkhausen voltage in astm a36 steel. *IEEE Transactions on Magnetics*, 49(7):4148–4151.

Kypris, O., Nlebedim, I. C., and Jiles, D. C. (2014). Barkhausen spectroscopy: Non-destructive characterization of magnetic materials as a function of depth. *Journal of Applied Physics*, 115(17):17E305.

Landau, L. L. E. (1935). On the theory of the dispersion of magnetic permeability in ferromagnetic bodies. In *Physik. Z. Sowjetunion*, volume 8, pages 153–169.

Liorzou, F., Phelps, B., and Atherton, D. (2000). Macroscopic models of magnetization. *IEEE Transactions on Magnetics*, 36(2):418–428.

Lyshevski, S. E. (2005). *Nano- and micro-electromechanical systems: Fundamentals of nano- and microengineering*, volume 8 of *Nano- and microscience, engineering, technology, and medicine series*. CRC Press, Boca Raton [u.a.], 2 edition.

Melikhov, Y. Y., Tomáš, I., Kadlecová, J., and Perevertov, O. V. (2000). Investigation of two-phase samples by preisach modelling. *Journal of magnetism and magnetic materials*, 215:27–29.

Mierczak, L., Jiles, D. C., and Fantoni, G. (2011). A New Method for Evaluation of Mechanical Stress Using the Reciprocal Amplitude of Magnetic Barkhausen Noise. *IEEE Transactions on Magnetics*, 47(2):459–465.

Mitra, A. and Jiles, D. (1995). Effects of tensile stress on the magnetic Barkhausen effect in 2605 CO amorphous alloy. *IEEE Transactions on Magnetics*, 31(6):4020–4022.

Preisach, F. (1935). Über die magnetische Nachwirkung. *Zeitschrift für Physik*, 94(5-6):277–302.

Raghunathan, A. (2010). *Growth,Characterization and Modelling of Novel Magnetic Thin Films for Engineering Applications*. PhD thesis, Cardiff University, Cardiff, UK.

Raghunathan, A., Klimczyk, P., and Melikhov, Y. (2013). Application of Jiles-Atherton Model to Stress Induced Magnetic Two-Phase Hysteresis. *IEEE Transactions on Magnetics*, 49(7):3187–3190.

Raghunathan, A., Melikhov, Y., Snyder, J., and Jiles, D. (2012). Modeling of two-phase magnetic materials based on Jiles–Atherton theory of hysteresis. *Journal of Magnetism and Magnetic Materials*, 324(1):20–22.

Roy, R. K., Panda, A. K., and Mitra, A. (2012). An electromagnetic sensing device for microstructural phase determination of steels through non-destructive evaluation. In *Sensing Technology (ICST), 2012 Sixth International Conference on*, pages 226–229. IEEE.

Sablik, M. and Jiles, D. (1993). Coupled magnetoelastic theory of magnetic and magnetostrictive hysteresis. *IEEE Transactions on Magnetics*, 29(4):2113–2123.

Stoner, E. W. E. (1948). A mechanism of magnetic hysteresis in heterogeneous alloys. In *Philosphical Transactions of the Royal Society of London*, pages 599–642.

Tumanski, S. (2007). Induction coil sensors—a review. *Measurement Science and Technology*, 18(3):R31–R46.

Umenei, A. E., Melikhov, Y., and Jiles, D. C. (2011). Analytic Solution for Variations of Magnetic Fields in Closed Circuits: Examination of Deviations From the Standard Ampere's Law Equation. *IEEE Transactions on Magnetics*, 47(4):734–737.

Wilson, J. S. (2005). *Sensor technology handbook*. Elsevier, Amsterdam and Boston.

Wilson, P., Ross, J., and Brown, A. (2002). Simulation of magnetic component models in electric circuits including dynamic thermal effects. *IEEE Transactions on Power Electronics*, 17(1):55–65.